Article:
Edmans, J.G. orcid.org/0000-0002-4539-9145, El-Howati, A., Slowik, K.M. et al. (4 more authors) (2025) pH-responsive diblock copolymer vesicles via polymerization-induced self-assembly in aqueous media: synthesis, loading, and potential biological applications. ACS Applied Materials & Interfaces, 17 (24). pp. 35140-35154. ISSN 1944-8244

https://doi.org/10.1021/acsami.5c05091

pH-responsive diblock copolymer vesicles via polymerization-induced self-assembly in aqueous media: synthesis, loading and potential biological applications

Jake G. Edmans[a,b], Asma El-Howati[b], Klaudia M. Slowik[b], Helen E. Colley[b,c] *, Craig Murdoch[b,c], Paul V. Hatton[b,c] and Steven P. Armes[a] *

a. Dainton Building, School of Mathematical and Physical Sciences, University of Sheffield, Brook Hill, Sheffield, South Yorkshire, S3 7HF, UK.

b. School of Clinical Dentistry, University of Sheffield, 19 Claremont Crescent, Sheffield, South Yorkshire, S10 2TA, UK.

c. Insigneo Institute, Sheffield, UK, The Pam Liversidge Building, Sheffield S1 3JD.

Abstract. Polymerization-induced self-assembly (PISA) offers a useful strategy for the efficient encapsulation of biomacromolecules within diblock copolymer vesicles under mild conditions. This approach eliminates the need for a separate vesicle loading step and should be particularly advantageous for drug delivery applications if suitable biocompatible vesicles can be designed to release their encapsulated cargo in response to a specific environmental stimulus. Ideally, the vesicles should remain intact after endocytosis but subsequently undergo dissociation when exposed to the mildly acidic conditions (pH ~ 5) found within intracellular endosomal compartments of mammalian cells. In this study, reversible addition-fragmentation chain-transfer (RAFT) aqueous dispersion copolymerization of 2-hydroxypropyl methacrylate (HPMA) and 2-*N*-(morpholino)ethyl methacrylate (MEMA) was conducted using a water-soluble poly(glycerol monomethacrylate) (PGMA) precursor to prepare a series of PGMA-*b*-P(HPMA-*stat*-MEMA) copolymer vesicles. Such vesicles exhibit tunable pH-responsive behavior, leading to their dissociation between pH 3.5 and pH 6 depending on their MEMA content. F(ab) antibody fragments were loaded within these vesicles during their aqueous PISA at 45 °C with an encapsulation efficiency of 42 ± 4 %: this antibody retains its antigen-binding functionality and is subsequently released from the vesicles at pH ≤ 5.25. Furthermore, nano-flow cytometry (NanoFCM) analysis confirms the encapsulation of plasmid DNA within these vesicles and their subsequent take-up by human keratinocytes highlights the versatility of this technique for biotherapeutic delivery. This is the first reported example of PISA being used to prepare vesicles loaded with either antibody fragments or nucleic acids that can be subsequently released under physiologically relevant conditions, without requiring additional reactions or post-polymerization loading steps. In principle, encapsulation of proteins, antibodies, enzymes or oligonucleotides within vesicles during their PISA synthesis has the potential to significantly advance nanomedicine.

* Corresponding authors: s.p.armes@sheffield.ac.uk or h.colley@sheffield.ac.uk

Keywords: Polymerization-induced self-assembly, pH-responsive, copolymers, polymer vesicles, polymersomes, drug delivery, antibody, DNA

Introduction

Over the past few decades, the self-assembly of pH-responsive block copolymers in aqueous media has attracted considerable attention.[1–5] There has been particular interest in the design of block copolymer vesicles (a.k.a. polymersomes) that undergo dissociation under physiologically relevant conditions.[6–11] This is because such vesicles can be loaded with therapeutic agents for delivery into mammalian cells.[7–9] However, the efficient loading of proteins or nucleic acids (e.g. DNA, mRNA) within diblock copolymer vesicles under mild conditions remains technically challenging.[12,13] Film rehydration and similar top-down methods are slow and inefficient for loading large biomacromolecules into vesicles during self-assembly.[9,13–15] Nanoprecipitation methods based on water-miscible organic solvents such as tetrahydrofuran are rarely used to load such cargoes owing to their poor solubility and denaturation. [12, 16–20] Furthermore, all traces of any organic cosolvent would need to be carefully removed by exhaustive dialysis or freeze-drying. The pH switch method has been used to load poly(2-(methacryloyloxy)ethyl phosphorylcholine)-poly(2-(diisopropylaminoethyl methacrylate) vesicles with an encapsulation efficiency of approximately 20% for DNA and 10% for antibodies.[8,21–23] Electroporation has also been used to load biomacromolecules within such vesicles. [24,25] However, encapsulation efficiencies were typically less than 10% and some biomacromolecules may undergo partial degradation at the relatively high voltages required for this technique.

Polymerization-induced self-assembly (PISA) is a powerful platform technology for the efficient synthesis of a wide range of block copolymer nano-objects in the form of concentrated colloidal dispersions.[26,27] When conducted in aqueous media, PISA involves growing a water-insoluble block from one end of a water-soluble block to produce an amphiphilic diblock copolymer.[28] At a certain critical degree of polymerization (DP) for the hydrophobic block, *in situ* self-assembly occurs to produce nascent nanoparticles, initially with a spherical morphology. Depending on the target

diblock copolymer composition (and various other synthesis parameters), the final morphology can be spheres, worms or vesicles.[29] Recently, there has been considerable interest in the use of aqueous PISA for the encapsulation of drugs and biomacromolecules within vesicles for drug or vaccine delivery.[30–33] Of particular relevance to the present study, PISA can be performed under sufficiently mild conditions to enable the *in situ* encapsulation of proteins or DNA within copolymer vesicles without inducing their denaturation.[32,34–40] Herein we report the synthesis of new pH-responsive vesicles via statistical copolymerization of 2-*N*-(morpholino)ethyl methacrylate (MEMA) with 2-hydroxypropyl methacrylate (HPMA) using a reversible addition-fragmentation chain transfer (RAFT) aqueous dispersion polymerization formulation (**Scheme 1**).

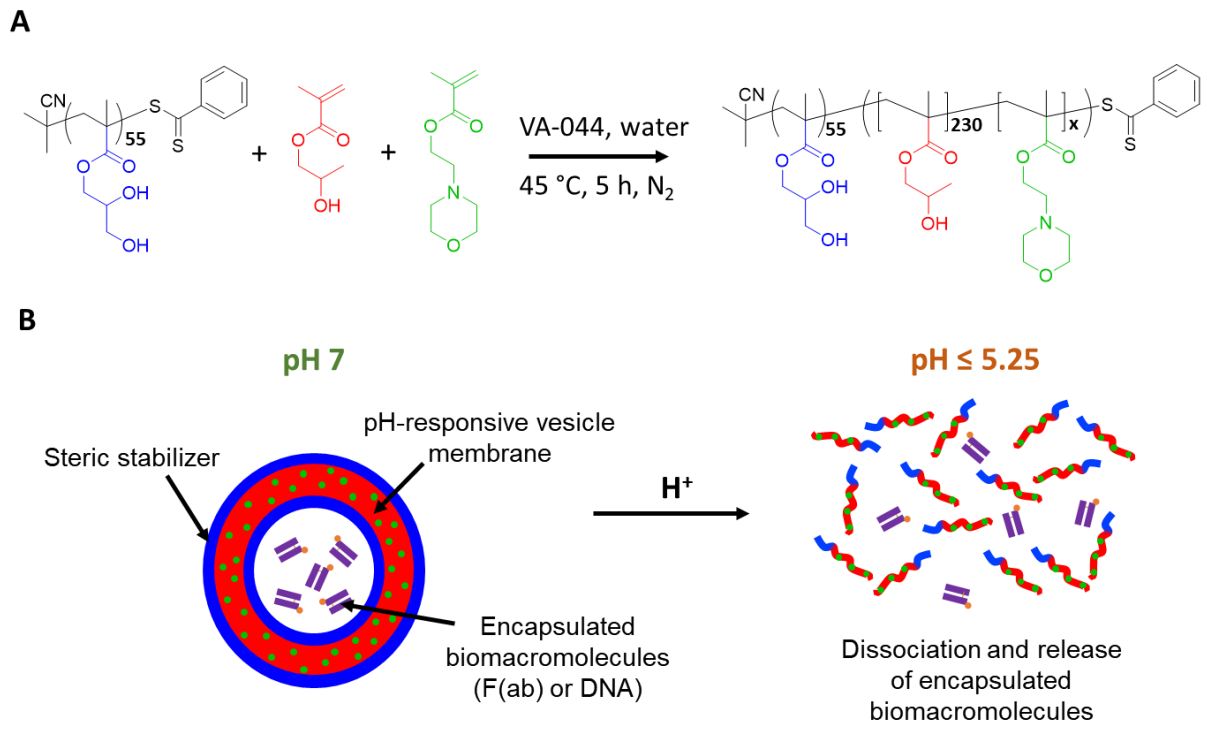

Scheme 1. (A) Scheme for the synthesis of PGMA-P(HPMA-*stat*-MEMA) diblock copolymer vesicles via RAFT aqueous dispersion copolymerization of HPMA with MEMA whereby the latter comonomer repeat units are randomly distributed throughout the hydrophobic block. (B) Biomacromolecules can be encapsulated within such vesicles during their PISA synthesis at 45 °C and are subsequently released on lowering the dispersion pH owing to protonation of the pendent morpholine groups, which induces vesicle dissociation.

MEMA is a hydrophilic monomer so its incorporation into the membrane-forming block must be relatively limited, otherwise there would be no *in situ* self-assembly in aqueous media. Accordingly, the MEMA content of the membrane-forming block was systematically varied from zero to 14.8 mol% and the pH-responsive behavior of the resulting vesicles examined. An optimized diblock copolymer composition was identified for the relatively efficient encapsulation and release of F(ab) antibody fragments, which served as a model functional biomacromolecule. Finally, the loading of plasmid DNA within vesicles and delivery into cells was demonstrated.

Experimental Section

Materials

Glycerol monomethacrylate (GMA) was donated by GEO Specialty Chemicals (Hythe, UK). 2-hydroxypropyl methacrylate (HPMA; mixture of isomers, ≥ 97%) was purchased from Alfa Aesar, UK. 2-(*N*-Morpholino)ethyl methacrylate) (MEMA; ≥ 95%) and 2-(methacryloxy)ethyl thiocarbamoyl rhodamine B were purchased from Polysciences (Germany). 2,2'-azobis[2-(2-imidazolin-2-yl)propane]dihydrochloride (VA-044) was purchased from Wako Specialty Chemicals (Germany). Ethanol, dichloromethane (DCM; 99.8%), and dimethylformamide (DMF; ≥ 99.7%) were purchased from ThermoFisher (Loughborough, UK). Bovine serum albumin (BSA), 4'-azobis-4- cyanopentanoic acid (ACVA; ≥ 98%), 2-cyano-2-propyl benzodithioate (CPDB; ≥ 97%), d_4-methanol, d_6-acetone, buffer salts, and all cell culture reagents were purchased from Sigma Aldrich (Gillingham, UK). Mouse IgG, biotinylated goat anti-mouse F(ab) [B-F(ab)] and Texas Red-labeled F(ab) [TxR-F(ab)] were purchased from Abcam (Cambridge, UK). Other enzyme-linked immunosorbent assay (ELISA) reagents were purchased from Biotechne (Abingdon, UK). The mCherry2-C1 plasmid was a gift from Michael Dawson (Addgene plasmid #54563). Deoxyribonucleotide triphosphate (dNTP) mixes,

lipofectamine™, and PicoGreen™ were purchased from ThermoFisher Scientific (Loughborough, UK). Sephacryl S-500 HR was purchased from Cytiva (Amersham, UK).

Synthesis of the PGMA precursor

This synthesis was based on a literature protocol.[34] A round-bottomed flask was charged with GMA (30.0 g; 187 mmol), CPDB (0.829 g; 3.75 mmol; target degree of polymerization, DP, = 50), ACVA (0.167 mg; 0.596 mmol; CPDB/ACVA molar ratio = 6.3), and ethanol (40.0 g), and then sealed using a rubber septum. This reaction vessel was purged with N_2 gas for 30 min and placed in a pre-heated oil bath at 70 °C for 3 h, after which the polymerization was quenched by immersing the flask in an ice bath while exposing its contents to air. The resulting PGMA precursor (GMA conversion = 86%, **Figure S1**; M_n = 14,200 g mol^{-1}, M_w/M_n = 1.16, **Figure S2**) was purified by precipitation into excess DCM to remove unreacted monomer and initiator residues. A mean degree of polymerization (DP) of 55 was calculated using ^{1}H NMR spectroscopy (d_4-methanol) by comparing the integrated signals between 3.4 ppm and 4.3 ppm assigned to the five pendant group protons of the GMA repeat units with that of the five aromatic protons between 7.4 ppm and 8.0 ppm assigned to the dithiobenzoate end-group (**Figure S3**).[34]

Synthesis of pH-responsive diblock copolymer vesicles via RAFT aqueous dispersion copolymerization of HPMA with MEMA

$PGMA_{55}$-P($HPMA_{230}$-*stat*-$MEMA_{30}$) (G_{55}-(H_{230}-*stat*-M_{30}) was synthesized as follows. HPMA (0.367 g; 2.55 mmol), MEMA (66.2 mg, 0.332 mmol) and the $PGMA_{55}$ precursor (0.100 g; 11.1 µmol; target degree of polymerization = 260), were dissolved in deionized water (1.94 g) in a sealed glass vial and purged with N_2 gas for 20 min. VA-044 initiator (0.20 mL of a 3.50 g dm^{-3} aqueous solution; 2.16 µmol; $PGMA_{55}$/VA-044 molar ratio = 5.1) was added and the reaction solution purged for a further 10 min prior to immersing the vial in an oil bath set at 45 °C for 18 h. The masses of MEMA and

deionized water were adjusted as required to target the desired P(HPMA-*stat*-MEMA) DP at 20% w/w solids **(Table S1)**. The copolymerization was quenched by exposing the reaction mixture to air, followed by dilution to 10% w/w solids using deionized water and cooling to 20 °C. The final comonomer conversion was determined by ^{1}H NMR spectroscopy analysis (d_4-methanol) as previously described.[34] Very weak vinyl signals at 5.6 and 6.2 ppm indicated a final overall comonomer conversion of > 99% (**Figure S4**). To prepare B-F(ab)-loaded vesicles, B-F(ab) (50.0 μg) and BSA (20.0 mg) were added to the reaction mixture and the reaction time was reduced to 5 h. To prepare TxR-F(ab) loaded vesicles, TxR-F(ab) (500.0 ug) and BSA (20.0 mg) were added to the reaction mixture and the reaction time was reduced to 5 h. To prepare rhodamine B (Rh)-labeled fluorescent vesicles, 2-(methacryloxy)ethyl thiocarbamoyl rhodamine B (0.74 mg, 1.1 μmol) was added to the reaction mixture and the reaction time was reduced to 5 h. To prepare Rh-labeled and plasmid-loaded vesicles, 2-(methacryloxy)ethyl thiocarbamoyl rhodamine B (0.74 mg, 1.1 μmol), dNTP (1.5 μM), and purified mCherry plasmid (120 μL at 2 μg/μL) were added to the reaction mixture and the reaction time was reduced to 5 h.

Characterization Techniques

NMR Spectroscopy

All ^{1}H NMR spectra were recorded using a 400 MHz Bruker Avance-400 spectrometer operating at 293 K with 64 scans being averaged per spectrum.

Gel Permeation Chromatography (GPC)

Copolymer solutions were analyzed at approximately 0.5 % w/w in HPLC-grade DMF (0.80 g dm^{-3} LiBr) and passed through a 0.45 μm polytetrafluoroethylene filter. Analysis was performed using a GPC instrument comprising an Agilent 1260 Infinity series degasser and pump, an Agilent PL-gel guard column, two Agilent Mixed-C columns, a refractive index detector and a UV detector set at a

wavelength of 305 nm. Calibration was achieved using eleven near-monodisperse poly(methyl methacrylate) standards ranging from 2.38 × 10^2 to 2.20 × 10^6 g mol^{-1}. Molecular weights and dispersities were calculated using Agilent GPC software.

Dynamic Light Scattering (DLS)

The hydrodynamic z-average diameter (D_z) and polydispersity index (PDI) were determined at 25 °C via the Stokes-Einstein equation using a Malvern Zetasizer NanoZS instrument. The cumulants method was used and a refractive index of 1.59 was assumed. Hydrodynamic number-average diameters (D_n) were also calculated in some experiments. All measurements were performed on 0.10% w/w copolymer dispersions using disposable plastic cuvettes and all data were averaged over three consecutive runs.

Acid titration

Continuously stirred 2.0% w/w copolymer dispersions were titrated with 10 mM HCl using a micropipet while recording the solution pH using a calibrated Thermo Scientific Orion Star A series pH meter. Equivalence points were determined using GraphPad Prism software as the minima of the first derivative of the titration curves. The apparent pK_a is defined as the pH at the half-equivalence point.[41]

Transmission Electron Microscopy (TEM)

Copper/palladium TEM grids (Agar Scientific, UK) were coated in-house to deposit a thin film of amorphous carbon and then subjected to a plasma glow discharge for 30 s. A micropipet was used to place one 10 µL droplet of a 0.10% w/w aqueous copolymer dispersion on a freshly treated grid for 1 min and the excess fluid was removed by washing twice with 10 µL water droplets for 20 s. To ensure sufficient electron contrast, MEMA-based nanoparticles were stained by the sequential

placement of two 10 µL droplets of a 1.0% w/w aqueous solution of phosphotungstic acid on the surface of each TEM grid for 20 s. For nanoparticles containing no MEMA comonomer, staining was achieved by sequential placement of two 10 µL droplets of a 0.75 % w/w aqueous solution of uranyl formate on the surface of each TEM grid for 20 s. Each grid was then carefully dried using a vacuum hose. Imaging was performed using a FEI Tecnai Spirit 2 microscope operating at 80 kV and equipped with an Orius SC1000B camera. Images were processed using *ImageJ* software.[42]

Turbidimetry experiments

Copolymer dispersions were prepared at 0.1% w/v in 0.1 M sodium citrate (pH 3 – 6) or potassium phosphate (pH 6.25 – 8) buffers. To measure the dispersion turbidity, 100 µL aliquots were transferred to a 96-well plate in duplicate and their absorbance (or optical density, OD) was determined at 600 nm using a Tecan microplate reader.

Aqueous electrophoresis

A Malvern Zetasizer NanoZS instrument was used to determine electrophoretic mobilities at 25 °C. These measurements were performed on 0.10% w/w aqueous dispersions containing 10 mM KCl as background electrolyte, with the dispersion pH being adjusted using either dilute HCl or NaOH as required. Zeta potentials were calculated from the Henry equation using the Smoluchowski approximation.

Quantification of pH-induced F(ab) release

A biotinylated polyclonal goat anti-mouse F(ab) (B-F(ab)) was used as a model protein to assess the extent of encapsulation of biomacromolecules within diblock copolymer vesicles and their subsequent pH-triggered release. A direct enzyme-linked immunosorbent assay (ELISA) was used to quantify the concentration of free (non-encapsulated) biotinylated goat anti-mouse F(ab), as

previously described.[32,43] Dilute (2.0% w/v) copolymer dispersions were diluted ten-fold by volume via pipet using either 0.1 M aqueous buffers of varying pH (pH 7, potassium phosphate; pH 3-6, sodium citrate) or ethanol for 5 to 10 seconds before immediately diluting one hundred-fold using PBS buffer (pH 7.4) prior to the ELISA determination of antigen binding activity.

The encapsulation efficiency was determined for unpurified formulations by comparing analyte levels for both intact and ethanol-treated samples to determine the amount of encapsulated payload by difference.[44] The payload is released on exposure to ethanol because this is a good solvent for the membrane-forming copolymer chains, whereas exposure to potassium phosphate buffer (pH 7) leaves the vesicles intact (i.e. no payload release). The concentration of encapsulated F(ab) was calculated from ELISA measurements by subtracting the concentration of unencapsulated F(ab) (following exposure to pH 7 buffer) from the total F(ab) concentration (following exposure to ethanol), as shown in equation (1).

$$[F(ab)]_{encapsulated} = [F(ab)]_{total} - [F(ab)]_{unencapsulated} \quad (1)$$

The percentage encapsulation efficiency (%EE) achieved during the vesicle synthesis was calculated using equation (2) by normalizing the ELISA measurement of encapsulated F(ab) concentration relative to the maximum theoretical concentration based on the amount of F(ab) added to the reaction mixture. In addition, the percentage loss in antigen-binding activity (%AL) during synthesis was calculated using equation (3).

$$\%EE = 100 \times \frac{[F(ab)]_{encapsulated}}{[F(ab)]_{max}} \quad (2)$$

$$\%AL_{synthesis} = 100 \times \left(1 - \frac{[F(ab)]_{total}}{[F(ab)]_{max}}\right) \quad (3)$$

Finally, the percentage release achieved in response to exposure to a given pH ($\%Release_{pHx}$) was calculated using equation (4) by normalizing relative to the extent of ethanol-induced release.

$$\%Release_{pHx} = 100 \times \frac{[F(ab)]_{pHx} - [F(ab)]_{unencapsulated}}{[F(ab)]_{encapsulated}} \quad (4)$$

Encapsulation and subsequent release and quantification were performed four times (N = 4).

Preparative size exclusion chromatography experiments

Aqueous dispersions of either Texas Red-loaded or empty G_{55}-(H_{230}-*stat*-M_{30}) vesicles (0.50 mL, 10% w/w) were fractionated by preparative size exclusion chromatography (SEC) using 20 mL of Sephacryl S-500 HR resin with PBS as the mobile phase, with multiple fractions of approximately 200 µL per fraction being collected. 100 µL of each fraction was transferred to a black, transparent-bottom 96-well plate before measuring absorbance (or optical density, OD) at 600 nm using a Tecan microplate reader. Then ethanol (100 µL) was added to each well to induce vesicle dissociation, thereby releasing the vesicle payload and producing a transparent solution. Fluorescence was subsequently measured at an emission wavelength of 615 nm (excitation wavelength = 596 nm) using the same microplate reader. Identical acquisition settings (including gain) were used for all fluorescence measurements.

Nano-flow cytometry analysis of plasmid DNA encapsulation and release

Either empty or DNA-loaded Rhodamine B-labeled vesicles were diluted to 0.1% w/v in deionized water. In this case, 0.25% v/v PicoGreen solution was added as required and the resulting

dispersions were incubated for 18 h in the dark to enable this dye to permeate the vesicle membrane and bind to DNA. Then each vesicle dispersion was diluted one hundred-fold using deionized water immediately prior to nano-flow cytometry (NanoFCM) analysis. Acid (1 µL of 1 M HCl) was added to 100 µL of such dilute dispersions to trigger their dissociation immediately prior to analysis. Rh-labeled vesicles and PicoGreen-stained DNA were detected using a 488 nm laser combined with 525/40 and 585/40 nm bandpass filters, respectively. Scattering intensity and fluorescence measurements were recorded for 1 min per sample and the particle size was interpolated from a standard scattering intensity curve constructed for near-monodisperse silica nanoparticles, as recommended by the manufacturer.

Vesicle-mediated DNA delivery to oral keratinocytes

Vesicles loaded with plasmid DNA were prepared at 0.1% w/w in PBS containing 0.25 % v/v PicoGreen solution and incubated for 18 h in the dark to enable this dye to permeate the vesicle membrane and stain the DNA. The vesicles were sedimented by centrifuging at 200 g for 5 min before discarding the supernatant and resuspending the vesicles in cell culture medium at 0.1 % w/v. FNB6-hTERT immortalised oral keratinocytes (FNB6; Ximbio) were cultured in a flavin- and adenine-enriched medium consisting of high glucose Dulbecco's modified Eagle's medium (DMEM) and Ham's F12 medium in a 3:1 v/v ratio supplemented with 10% v/v foetal bovine serum (FBS), epidermal growth factor (10 ng/mL), adenine (0.18 mM), insulin (5 µg/mL), transferrin (5 µg/mL), L-glutamine (2 mM), triiodothyronine (0.2 nM), amphotericin B (0.625 µg/mL), penicillin (100 IU/mL), and streptomycin (100 µg/mL).[45] Then 1 x 10^5 cells in 1.5 mL cell culture medium per dish were seeded in µ-Dish 35 mm, high Glass Bottom microscopy dishes (Ibidi GmbH, Germany) and allowed to adhere overnight. The media were replaced with fresh media containing 0.1 % w/v vesicles for 1 h before washing three times with PBS. Cell nuclei were stained using Hoechst 33342 and acidic intracellular organelles using LysoTracker Deep Red (ThermoFisher Scientific, UK), as recommended

by the manufacturer. Cells were subsequently imaged using a Zeiss LSM880 AiryScan confocal microscope where images were acquired in three-channel mode and 2D AiryScan processing was applied prior to image analysis using *ImageJ* software.[42]

For transfection experiments, 5 x 10^4 FNB6 cells per well were seeded in a 96-well plate, allowed to adhere overnight then incubated with 1 % w/v vesicles in cell culture medium. After 24 h, cells were washed three times with PBS and imaged using a Bio-Rad ZOE fluorescent imager. As a positive control, cells were transfected with the plasmid at 2 μg/μL using lipofectamine (ThermoFisher Scientific, UK) according to the manufacturer's instructions and then cultured overnight.

Results and Discussion

Synthesis of pH-responsive diblock copolymer vesicles

A water-soluble poly(glycerol monomethacrylate) precursor with a mean degree of polymerization of 55 (hereby denoted G_{55}) was prepared by RAFT solution polymerization in ethanol at 70 °C (**Figures S1-S3**).[34] This precursor was chain-extended via statistical copolymerization of HPMA with varying amounts of MEMA using a RAFT aqueous dispersion polymerization formulation at 45 °C for 18 h to produce a series of diblock copolymer vesicles at 20% w/w solids (**Scheme 1A**). Such vesicles are hereafter denoted as G_{55}-(H_{230}-*stat*-M_x), where x is the target number of MEMA repeat units per copolymer chain (**Table 1**). ^{1}H NMR spectroscopy analysis of the final reaction mixtures in d_4-methanol confirmed that the final comonomer conversion was more than 99% for each target copolymer composition (**Figure S4**). ^{1}H NMR spectra recorded for purified copolymers revealed characteristic signals assigned to the MEMA repeat units at 2.6 and 2.7 ppm (**Figure 1** and **Figure S5**), which were used to determine copolymer compositions. According to this analysis, the MEMA content ranged from 0 to 14.8 mol% for these copolymers (**Figure S5**).

Table 1. Summary of NMR, GPC, DLS, acid titration and turbidimetry data obtained for a series of G_{55}-(H_{230}-*stat*-M_x) vesicles.

	MEMA content mol% [a]	GPC molecular weight data [b]		DLS data [c]			pK_a [d]	Dissociation pH [e]
		M_n (g mol^{-1})	M_w/M_n	D_n / nm	D_z / nm	PDI		
X = 0	0.0	62300	1.21	188	300	0.26	-	-
X = 10	3.8	70300	1.23	230	334	0.22	4.3	3.5-4
x = 20	8.1	72000	1.30	222	315	0.26	4.7	4.75-5
x = 30	11.1	74900	1.28	227	286	0.13	4.7	5.25-5.5
x = 40	14.8	70800	1.34	288	356	0.16	4.8	5.75-6

a. The MEMA content (mol%) was determined by ^{1}H NMR spectroscopy in d_4-methanol.

b. Number-average molecular weight (M_n) and dispersity (M_w/M_n) data were obtained by DMF GPC analysis using a refractive index detector and are expressed relative to near-monodisperse poly(methyl methacrylate) calibration standards.

c. Number-average (D_n), z-average (D_z) hydrodynamic diameters and polydispersity indices (PDI) were determined for 0.1% w/v aqueous copolymer dispersions using DLS.

d. The apparent pK_a (pK_a) was determined for each MEMA-based diblock copolymer based on the half-equivalence point of an acid titration against 10 mM HCl.

e. The critical pH range required for vesicle dissociation is defined as that in which the turbidity (as measured by the optical density recorded at 600 nm) is reduced to less than half that of the same dispersion at pH 7.

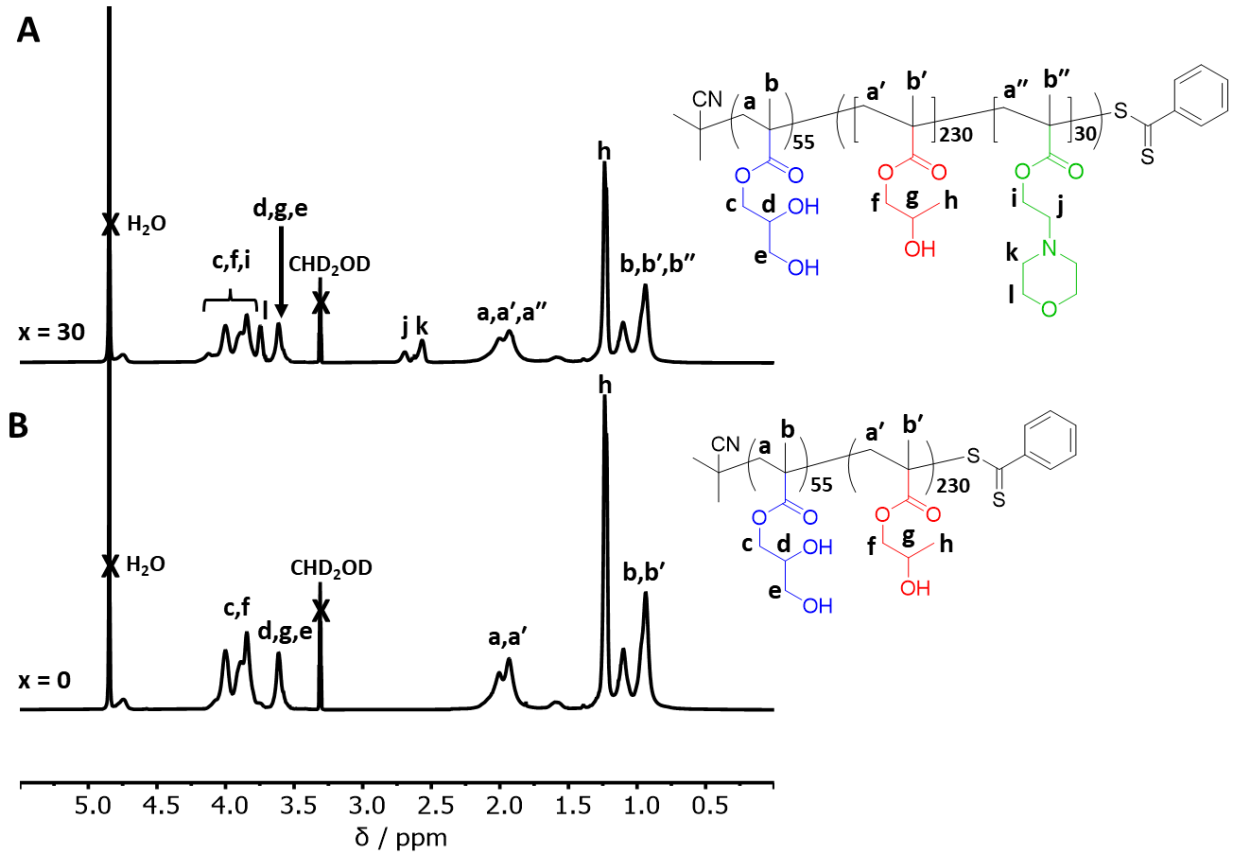

Figure 1. Assigned ^{1}H NMR spectra (d_4-methanol) recorded for (A) G_{55}-(H_{230}-*stat*-M_{30}) and (B) G_{55}-H_{230} diblock copolymers.

DMF GPC studies indicated that the apparent copolymer M_n increased from 62 300 to 74 900 g mol^{-1} when targeting higher MEMA contents [e.g. x = 0 – 30 for G_{55}-(H_{230}-*stat*-M_x)], while dispersities remained relatively low (Đ < 1.30). However, targeting x = 40 produced a slightly higher Đ value of 1.34 and an M_n of 70 800 g mol^{-1} (**Figure S6**). TEM studies confirmed a well-defined vesicular morphology for this series of copolymers (**Figure S7**). DLS studies of dilute aqueous dispersions of vesicles conducted in deionized water indicated mean hydrodynamic diameters of 286 to 356 nm with DLS polydispersities (PDIs) of 0.13–0.26 (**Figure S8**).

Acid titrations of 2.0% w/v copolymer dispersions were performed using 10 mM HCl (**Figure S9**). As expected, the $G_{55}H_{230}$ diblock copolymer exhibited no detectable basic character because it contains no MEMA repeat units. In contrast, the G_{55}-(H_{230}-*stat*-M_{10}) diblock copolymer had an apparent pK_a

(pK_a) of 4.3 while G_{55}-(H_{230}-*stat*-M_{20}) and G_{55}-(H_{230}-*stat*-M_{30}) both exhibited pK_a values of around 4.7. G_{55}-(H_{230}-*stat*-M_{40}) had a pK_a of 4.8 and this copolymer was strongly self-buffering at around pH 5.1.

Effect of morpholine content on pH-responsive behavior of diblock copolymer vesicles

Aqueous dispersions of vesicles are turbid owing to strong light scattering. Hence the molecular dissolution of pH-responsive vesicles on lowering the pH can be monitored by the reduction in turbidity (or optical density). Accordingly, copolymer dispersions were prepared at 0.1% w/v in 0.1 M buffers of varying pH before determining their optical density at 600 nm (OD_{600}) (**Figure 2A)**. As expected, the initial OD_{600} obtained for the morpholine-free $G_{55}H_{230}$ dispersion remained unchanged on lowering the solution pH. In contrast, copolymers comprising 10, 20, 30 or 40 MEMA units per chain underwent acid-triggered vesicle dissociation at pH 4.0–4.25, 4.75–5.00, 5.25–5.50, or 5.75–6.00, respectively. Moreover, a significant *increase* in OD_{600} was observed prior to each morphological transition. This is particularly noticeable for G_{55}-(H_{230}-*stat*-M_{10}) but is also evident for the other three copolymers. This suggests that jellyfish-like intermediates are formed under such conditions.[46]

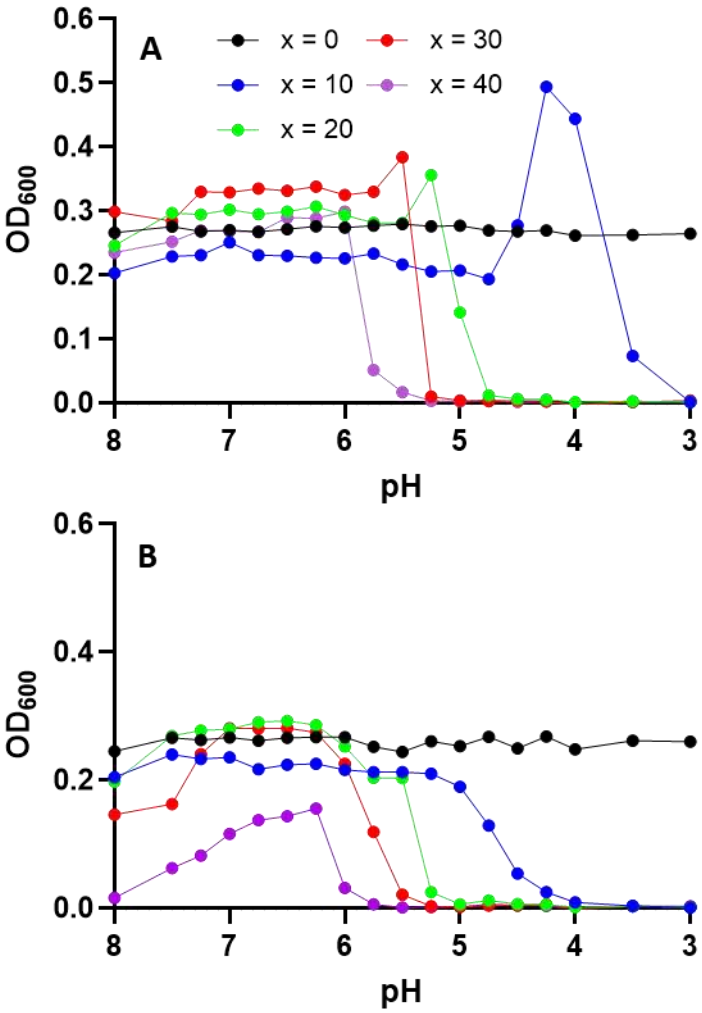

Figure 2. Effect of varying the dispersion pH on optical density (at λ = 600 nm) for a series of 0.1% w/v aqueous dispersions of G_{55}-(H_{230}-*stat*-M_x) vesicles prepared in 0.1 M buffers of varying pH: (A) determined immediately after preparation, (B) determined after storage of the same buffered solutions at 20 °C for 7 days.

To assess their colloidal stability, each of the buffered dispersions/solutions shown in **Figure 2A** were stored at 20 °C for 7 days before repeating the turbidimetry measurements (**Figure 2B**). The optical density observed for the G_{55}-(H_{230}-*stat*-M_{40}) vesicles was markedly lower across the entire pH range compared to the other four copolymer vesicles, suggesting relatively poor long-term colloidal stability in the presence of such buffers. In contrast, the turbidity observed for G_{55}-(H_{230}-*stat*-M_{30})

vesicles was only slightly lower after storage for 7 days at pH 6.25 – 7.00, suggesting a relatively high degree of colloidal stability in this case. Such colloidal (in)stability is also evident by visual inspection: G_{55}-(H_{230}-*stat*-M_{30}) vesicles remain turbid when dispersed in a pH 7 buffer but rapidly form a transparent solution in a pH 5 buffer owing to vesicle dissociation (**Figure S10**).

Diblock copolymer composition	Zeta potential / mV			
G_{55}-(H_{230}-*stat*-M_x)	pH 8	pH 7	pH 6	pH 5
X = 0	-10.6	-11.4	-6.2	-3.7
X = 10	-10.0	-8.0	+3.2	+17.8
X = 20	-16.4	-8.9	+3.7	+16.6
X = 30	-16.5	-10.9	+3.6	-
X = 40	-21.5	-8.6	+3.1	-

Table 2. Summary of zeta potential data obtained for a series of 0.1% w/v aqueous dispersions of G_{55}-(H_{230}-*stat*-M_x) vesicles in the presence of 0.01 M KCl background electrolyte.

Zeta potentials were determined as a function of pH for all five vesicle dispersions in the presence of 0.01 M KCl (**Table 2**). In each case, a weakly negative zeta potential was observed at or above pH 7 (ranging from –8.0 to –11.4 mV). The MEMA-free vesicles also exhibit a negative (albeit lower) zeta potential below pH 7. The four examples of G_{55}-(H_{230}-*stat*-M_x) vesicles (x = 10 to 40) each exhibited a slightly positive zeta potential of +3 to +4 mV at pH 6, indicating partial protonation of the pendent morpholine groups within the vesicle membranes. A significantly higher zeta potential was obtained at pH 5 for the G_{55}-(H_{230}-*stat*-M_{10}) and G_{55}-(H_{230}-*stat*-M_{20}) vesicles; this is close to the apparent pK_a determined by acid titration for these two copolymers, suggesting substantial protonation of the membrane-forming block. Finally, the G_{55}-(H_{230}-*stat*-M_{30}) and G_{55}-(H_{230}-*stat*-M_{40}) vesicles both become much less turbid at pH 5, preventing meaningful electrophoretic measurements.

pH-responsive behavior of optimized G_{55}-(H_{230}-*stat*-M_{30}) vesicles

Aqueous dispersions of pH-responsive G_{55}-(H_{230}-*stat*-M_{30}) and non-responsive $G_{55}H_{230}$ vesicles were prepared in 0.9% w/v NaCl (to simulate physiological conditions) before adjusting to either pH 7 or pH 4 prior to DLS studies. G_{55}-H_{230} vesicles exhibited a unimodal intensity-average particle size distribution and a z-average diameter of 310 nm (DLS PDI = 0.32), which remained essentially unchanged at 294 nm after pH adjustment (**Figure 3A**). The G_{55}-(H_{230}-*stat*-M_{30}) vesicles also exhibited a unimodal intensity-average particle size distribution at pH 7, with a z-average diameter of 389 nm (DLS PDI = 0.21) (**Figure 3B**). However, in this case a bimodal size distribution was observed at pH 4 comprising a major population at approximately 10 nm and a minor population at 80 nm. Given that DLS is strongly biased towards larger species,[47] this suggests that vesicle dissociation occurred under such conditions to form (mainly) molecularly-dissolved copolymer chains. Indeed, the corresponding number-average particle size distribution comprised solely molecularly-dissolved copolymer chains (**Figure 3C**).

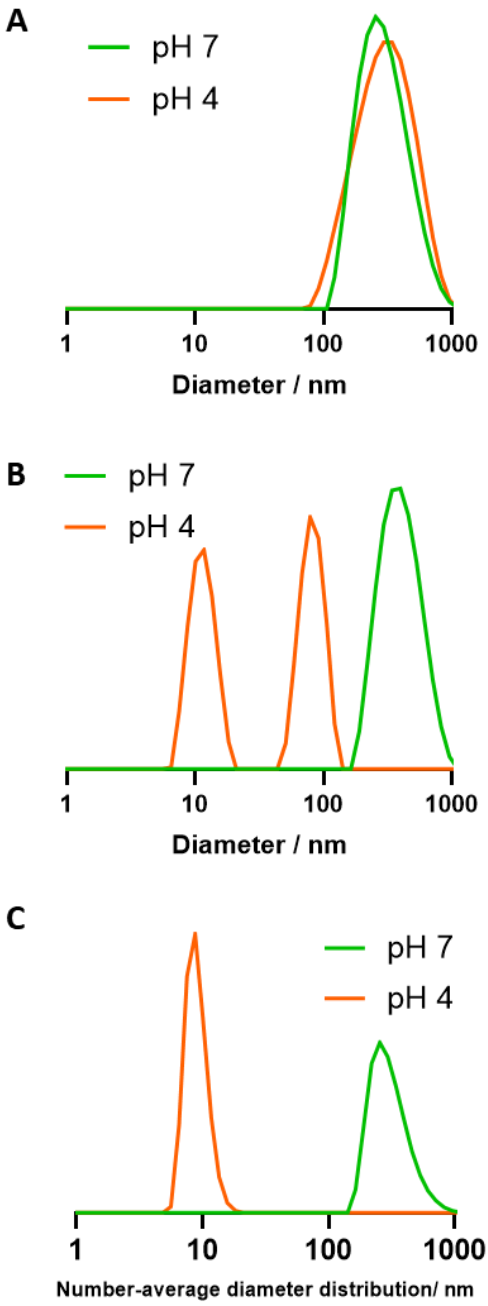

Figure 3. Intensity-average particle size distributions recorded by DLS in 0.9% w/v NaCl at pH 7 (green curves) and pH 4 (orange curves) for 0.1 % w/v aqueous dispersions of (**A**) $G_{55}H_{230}$ and (**B**) G_{55}-(H_{230}-*stat*-M_{30}). (**C**) Number-average particle size distributions recorded for G_{55}-(H_{230}-*stat*-M_{30}) at pH 4 (orange curve) and pH 7 (green curve).

G_{55}-(H_{230}-*stat*-M_{30}) vesicles were prepared in aqueous buffers of varying pH and visualized by TEM using phosphotungstic acid as a negative stain (**Figure 4**). A distinctive vesicular morphology is observed at either pH 7 or pH 6, with diameters of approximately 200-500 nm, similar to that

observed previously for $PGMA_{58}$-$PHPMA_{250}$ vesicles.[34] Very few (if any) colloidal structures were visible at pH 4 or pH 5, which is consistent with molecular dissolution of the copolymer chains under such conditions.

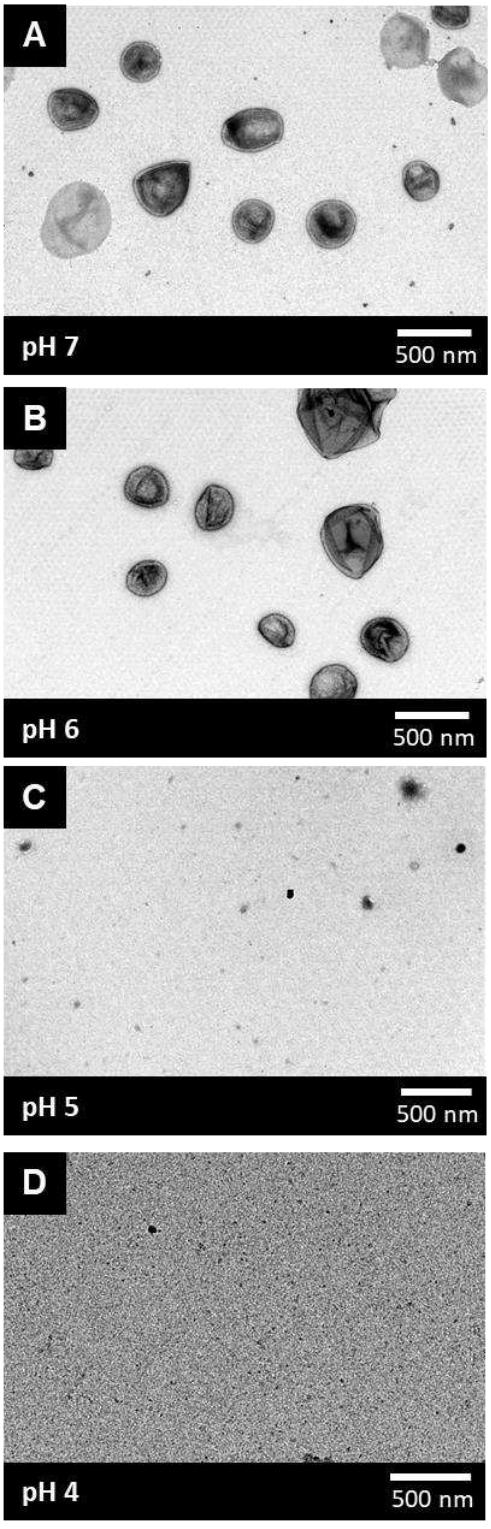

Figure 4. TEM images recorded for G_{55}-(H_{230}-*stat*-M_{30}) vesicles dispersed in 0.1 M aqueous buffers at (**A**) pH 7 (vesicles), (**B**) pH 6 (vesicles), (**C**) pH 5 (very few structures), (**D**) pH 4 (molecularly-dissolved copolymer chains). Scale bar = 500 nm in each case.

Aqueous dispersions of G_{55}-(H_{230}-*stat*-M_{30}) vesicles were prepared at 2.0% w/v in D_2O and the apparent pH was adjusted using 0.1 M DCl before recording ^{1}H NMR spectra (**Figure 5**). At pH 6-7, only weak signals are observed at 0.9 ppm and 3.6 – 4.1 ppm. The lack of a prominent peak at 1.3 ppm corresponding to the PHPMA pendant methyl group (**f**) indicates that these signals are caused by the polymer backbone methyl (**b**) and pendant glycerol (**c**, **d**, **e**) protons in the solvated PGMA stabilizer chains. Visual inspection confirmed that a transparent solution was formed at pH 5 and characteristic proton signals assigned to the protonated MEMA repeat units become visible under such conditions, indicating molecular dissolution of the copolymer chains. Importantly, the **j**, **k** (2.9 – 3.2 ppm), and **l** (3.9 ppm) proton signals have higher chemical shifts than those observed for the molecularly-dissolved copolymer in d_4-methanol (**Figure 1**). This is consistent with protonation of the pendent morpholine groups.[48,49] At pH 4, these **j**, **k**, and **l** signals are shifted further downfield as the degree of protonation of the morpholine group increases.

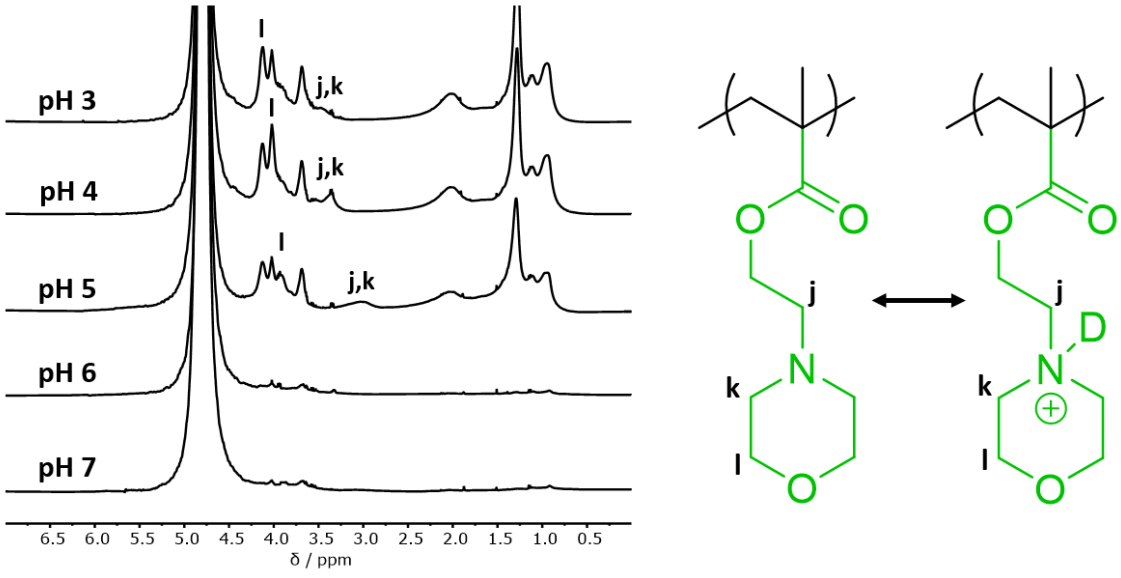

Figure 5. ^{1}H NMR spectra recorded for a G_{55}-(H_{230}-*stat*-M_{30}) diblock copolymer prepared at 2.0% w/v in DCl/D_2O at an apparent pH ranging from pH 3 to pH 7 with signals **j**, **k**, and **l** assigned to the pendent morpholine groups.

Copolymerization kinetics

Statistical copolymerization can produce random, gradient, or block-like copolymers depending on the relative reactivities of the two comonomers. To better understand its copolymer composition, G_{55}-(H_{230}-*stat*-M_{30}) was prepared in the presence of 3 mM sodium trimethylsilylpropanesulfonate, which serves as a convenient internal NMR standard. The reaction mixture was sampled at pre-determined timepoints for ^{1}H NMR analysis (after dilution with d_6-DMSO). The instantaneous HPMA conversion was calculated from the reduction in the methacrylic proton signal assigned to its predominant isomer at 6.10-6.15 ppm relative to that of the internal standard at 0 ppm (**Figure 6A**).[50]

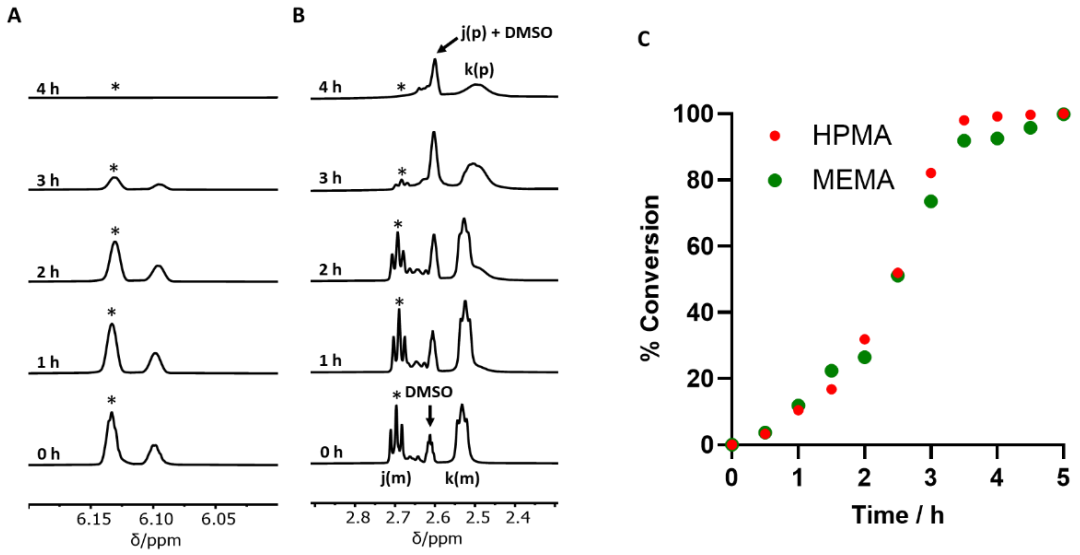

Figure 6. Kinetic data obtained for the statistical copolymerization of HPMA with MEMA during the synthesis of G_{55}-(H_{230}-*stat*-M_{30}) vesicles via RAFT aqueous dispersion polymerization at 45 °C when targeting 20 % w/w solids. The reaction mixture was sampled at predetermined timepoints for ^{1}H NMR spectroscopy studies after dilution in d_6-DMSO. (**A**) Partial ^{1}H NMR spectra illustrating the progressive reduction in the vinyl proton signal intensity over time. The signal assigned to the predominant HPMA isomer that is used to calculate the instantaneous conversion of this monomer is indicated by an asterisk. (**B**) Partial NMR spectra illustrating the reduction in the proton signals assigned to the MEMA monomer [denoted as **j(m)** and **k(m)**] over time. The former proton signal was used to calculate the instantaneous MEMA conversion. The signals associated with the MEMA polymer [**j(p)** and **k(p)**] occur at lower chemical shifts relative to the monomer, with the

j(p) signal overlapping with that of residual DMSO solvent. (**C**) Conversion vs. time curves determined for the consumption of HPMA and MEMA monomers, respectively.

Unfortunately, the methacrylic proton signal assigned to the copolymerized MEMA repeat units overlaps with those of the minor isomer of HPMA at 5.7 ppm. Hence the instantaneous MEMA conversion was monitored by comparing the integrated signal at 2.7 ppm assigned to the **j** protons of the MEMA monomer [denoted as **j(m)**] to that of the internal standard (**Figure 6B**). As the MEMA is consumed, the triplet **j** proton signal associated with the resulting copolymer chains [denoted as **j(p)**] broadens and shifts to 2.6 ppm, overlapping with the DMSO solvent peak. As expected for two methacrylic comonomers, HPMA and MEMA were consumed at comparable rates, with approximately 50% conversion being observed for both monomers after 2.5 h and more than 90% conversion after 3.5 h (**Figure 6C**). As is typically reported for RAFT aqueous dispersion polymerization formulations, the rate of (co)polymerization increases significantly following micellar nucleation, which occurs after approximately 2 h in this case.[46,51] Given that the relative rates of reaction of MEMA and HPMA are similar, the former comonomer is more or less randomly distributed throughout the hydrophobic membrane-forming block during the vesicle synthesis.

Encapsulation and pH-responsive release of F(ab) antibody fragments

F(ab) antibody fragments (~50 kDa) were used to investigate the vesicle encapsulation efficiency and subsequent pH-triggered release of a biologically-active protein. Biotinylated goat anti-mouse F(ab) was included in the initial reaction mixture along with bovine serum albumin (BSA), which acts as a stabilizing excipient. F(ab) was encapsulated within both morpholine-free vesicles [denoted F(ab)@G_{55}-H_{230}] and F(ab)@G_{55}-(H_{230}-*stat*-M_{30}) vesicles. A shorter reaction time of 5 h was used, as kinetic experiments (see Figure 6C) indicated that this should be sufficient to achieve full monomer conversion. Indeed, the presence of these proteins did not prevent very high comonomer conversions from being achieved during aqueous PISA, as indicated by the very weak methacrylic

monomer signals observed in ^{1}H NMR spectra recorded for each final reaction mixture (**Figure S11**). DMF GPC analysis indicated an M_n of 64 200 g mol^{-1} and an M_w/M_n of 1.22 for F(ab)@$G_{55}H_{230}$. Similarly, an M_n of 68 900 g mol^{-1} and an M_w/M_n of 1.26 was recorded for F(ab)@G_{55}-(H_{230}-*stat*-M_{30}) (**Figure S12**). TEM analysis confirmed that well-defined vesicles were obtained for both aqueous PISA formulations (**Figure S13**). The vesicle encapsulation efficiency was calculated using an enzyme-linked immunosorbent assay (ELISA) with immobilized mouse IgG.[32] The vesicles were diluted with ethanol to fully dissolve the copolymer chains, hence releasing the encapsulated protein (**Figure 7A**).

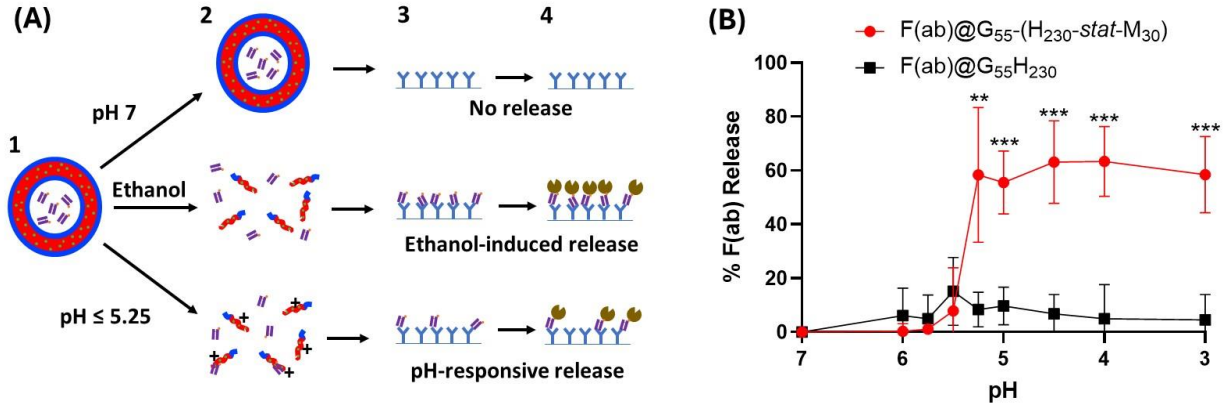

Figure 7. (**A**) Schematic diagram illustrating release of biotinylated goat anti-mouse IgG F(ab) antibody fragments from pH-responsive diblock copolymer vesicles after exposure to either low pH or ethanol. (**1**) F(ab) fragments are encapsulated *in situ* during the aqueous PISA synthesis of vesicles. (**2**) Vesicles undergo dissociation following exposure to either ethanol or a series of aqueous acidic buffers (pH ≤ 5.25), causing release of the encapsulated F(ab) fragments. (**3**) During an enzyme-linked immunosorbent assay (ELISA), the released F(ab) fragments bind to surface-immobilized mouse IgG. (**4**) Horseradish peroxidase enzyme is conjugated to the biotinylated F(ab), allowing quantification of the latter by colorimetric analysis. During its pH-triggered release, some of the F(ab) may form an ionic complex with the protonated diblock copolymer chains, which would result in a reduction in the antigen-binding functionality. (**B**) pH-triggered release of F(ab) from F(ab)@G_{55}-(H_{230}-*stat*-M_{30}) and F(ab)@$G_{55}H_{230}$ vesicles following exposure to aqueous buffers of varying pH. Dispersions were mixed briefly with the buffer prior to dilution with PBS (pH 7.4) and subsequent determination of the concentration of the released F(ab) by ELISA. Percentage of F(ab) release calculated by normalizing data relative to that obtained for ethanol-induced vesicle dissociation experiments. Data are presented as mean ± SD and statistical significance was determined by performing an unpaired t-test for each pH value with a significance difference indicated by **, $p < 0.01$; ***, $p < 0.001$.

ELISA analysis indicated that either 31 ± 6 % or 42 ± 4 % of the total F(ab) in the reaction mixture was encapsulated − and remained functional − within the F(ab)@$G_{55}H_{230}$ and F(ab)@G_{55}-(H_{230}-*stat*-M_{30}) vesicles, respectively. Moreover, 36 ± 7 % and 33 ± 9 % of the antigen-binding activity (N = 4) was lost following the PISA synthesis of the F(ab)@$G_{55}H_{230}$ and F(ab)@G_{55}-(H_{230}-*stat*-M_{30}) vesicles respectively, while the remaining F(ab) remained unencapsulated in the reaction mixture.

To confirm successful antibody encapsulation, Texas Red (TxR)-labeled F(ab) was encapsulated within G_{55}-(H_{230}-*stat*-M_{30}) vesicles, which were then fractionated via preparative size exclusion chromatography (SEC). Each fraction was analyzed by determining the optical density at 600 nm (OD_{600}) and fluorescence intensity at 615 nm to assess the vesicle and TxR-F(ab) concentrations, respectively. The first eluted fraction was both turbid and fluorescent: this indicates co-elution of TxR-F(ab) with the vesicles and provides strong evidence for successful encapsulation (**Figure S14A**). A second, broader fluorescent signal was also observed for later fractions; given its lack of associated turbidity, this latter signal is assigned to unencapsulated free F(ab). In a control experiment, empty G_{55}-(H_{230}-*stat*-M_{30}) vesicles were also subjected to SEC analysis. In this case, a similar OD_{600} signal was observed that overlapped with a relatively weak fluorescence signal owing to the intrinsic autofluorescence of the diblock copolymer (**Figure S14B**). In a second control experiment, a 10 % w/w aqueous dispersion of empty G_{55}-(H_{230}-*stat*-M_{30}) vesicles was incubated with the same concentration of TxR-F(ab) for 30 min at 20 °C prior to SEC analysis (**Figure S14C**). Again, a OD_{600} signal plus a corresponding weak fluorescence signal was initially observed, along with a relatively strong additional fluorescence signal associated with later (> 60) fractions that corresponds to free F(ab). These observations indicate that F(ab) is mainly encapsulated within the vesicles during PISA. Notwithstanding the autofluorescent nature of the copolymer vesicles, the possibility of a relatively low level of non-specific binding of F(ab) at the surface of the vesicles cannot be excluded.

To assess the efficacy of pH-triggered release, both types of F(ab)@loaded vesicles were mixed in turn with a series of 0.1 M aqueous buffers of varying pH prior to dilution using PBS (pH 7.4) and subsequent ELISA analysis (**Figure 7B**). The non-pH-responsive F(ab)@$G_{55}H_{230}$ vesicles exhibited minimal release of the encapsulated F(ab) protein, regardless of the solution pH. Similarly, no significant release was observed from the F(ab)-loaded G_{55}-(H_{230}-*stat*-M_{30}) vesicles at pH ≥ 5.5 but approximately 60% of the encapsulated F(ab) was released following exposure to a series of aqueous buffers ranging from pH 3.0 to 5.25.

Encapsulation of plasmid DNA

Diblock copolymer vesicles were labeled with rhodamine B (denoted as Rh hereafter) by incorporating a small amount of methacryloxyethyl thiocarbamoyl rhodamine B comonomer into the aqueous PISA formulation used to prepare G_{55}-(H_{230}-*stat*-M_{30}-*stat*-Rh) vesicles. Plasmid DNA was encapsulated within Rh-labeled vesicles by including this component in the aqueous PISA formulation used to produce the vesicles, which are denoted as DNA@G_{55}-(H_{230}-*stat*-M_{30}-*stat*-Rh). DNA encapsulation was confirmed by NanoFCM studies, which determines the fluorescence signal for *individual* vesicles. For such experiments, vesicles were treated with PicoGreen (a commercial fluorescent DNA stain) for 18 h at 20 °C to allow sufficient time for this fluorescent dye to permeate the vesicle membrane[36] and stain the encapsulated DNA prior to analysis.

In the absence of PicoGreen, both G_{55}-(H_{230}-*stat*-M_{30}-*stat*-Rh) and DNA@G_{55}-(H_{230}-*stat*-M_{30}-*stat*-Rh) vesicles displayed fluorescence arising from their rhodamine B comonomer but no fluorescence attributable to PicoGreen (**Figure 8A**-**B**).

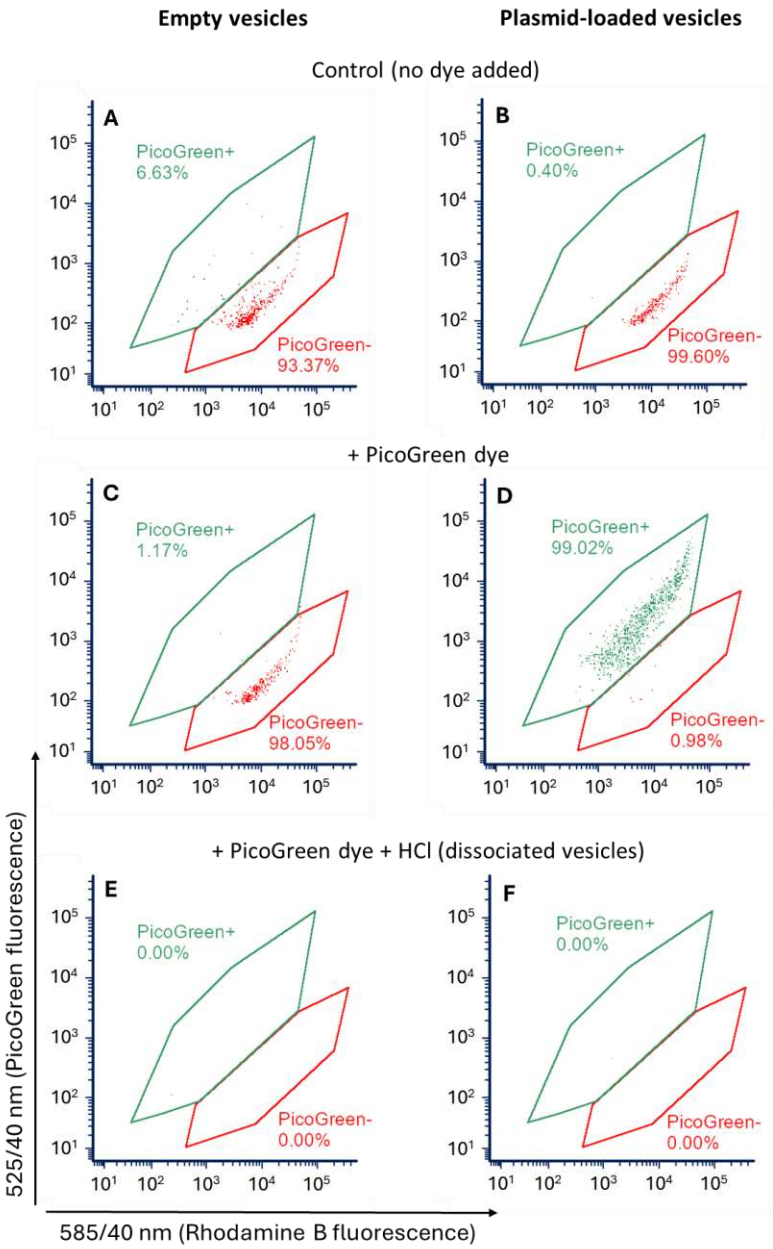

Figure 8. Single-particle analysis of PicoGreen-stained vesicles confirms their successful loading with plasmid DNA during PISA. Rhodamine B-labeled vesicles were treated with PicoGreen to stain their encapsulated DNA payload prior to their characterization using a nanoFCM flow analyzer equipped with a 488 nm blue laser. Scatter plots were constructed for the fluorescence intensity associated with rhodamine B and PicoGreen for each individual vesicle. Fluorescence scatter plots were recorded for empty G_{55}-(H_{230}-*stat*-M_{30}-*stat*-Rh) vesicles and DNA-loaded vesicles (denoted DNA@G_{55}-(H_{230}-*stat*-M_{30}-*stat*-Rh)) prepared using: (**A** & **B**) deionized water only, (**C** & **D**) PicoGreen fluorescence nucleic acid stain, and (**E** & **F**) following addition of 10 mM HCl. Gates indicate the relative number of PicoGreen-negative (red) and PicoGreen-positive (green) vesicles.

In the presence of PicoGreen, G_{55}-(H_{230}-*stat*-M_{30}-*stat*-Rh) vesicles alone displayed rhodamine fluorescence but no PicoGreen fluorescence, while DNA@G_{55}-(H_{230}-*stat*-M_{30}-*stat*-Rh) vesicles exhibited fluorescence originating from both rhodamine B and PicoGreen, indicating successful DNA encapsulation (**Figure 8C-D**). In this case, colocalization of fluorescence was observed for almost the entire vesicle population (~99%), suggesting that almost all of the vesicles contained DNA. Treatment of both G_{55}-(H_{230}-*stat*-M_{30}-*stat*-Rh) and DNA@G_{55}-(H_{230}-*stat*-M_{30}-*stat*-Rh) vesicles with HCl caused a dramatic reduction in light scattering events during NanoFCM analysis, indicating complete molecular dissolution, release of encapsulated DNA and therefore the pH-responsive character of such vesicles (**Figure 8E-F**).

Intracellular delivery of DNA

G_{55}-(H_{230}-*stat*-M_{30}-*stat*-Rh) or DNA@G_{55}-(H_{230}-*stat*-M_{30}-*stat*-Rh) vesicles were treated with PicoGreen for 18 h to stain encapsulated DNA before incubation with oral keratinocyte cells for 1 h. The nucleus and acidic organelles such as lysosomes or acidified endosomes within cells were subsequently stained using Hoechst 33342 and LysoTracker, respectively. Fluorescence images obtained by confocal microscopy showed that both empty and DNA-loaded vesicles were taken up by the cells and accumulated mostly in the perinuclear region (**Figure 9 B** & **H**). For cells exposed to G_{55}-(H_{230}-*stat*-M_{30}-*stat*-Rh), acidic organelles were sparse and distributed throughout cells, whereas the majority of acidic organelles were localized in the perinuclear region for cells exposed to DNA@G_{55}-(H_{230}-*stat*-M_{30}-*stat*-Rh) vesicles (**Figure 9 C** & **I**). Interestingly, the distribution of rhodamine-labeled copolymer did not fully overlap with acidic organelles, suggesting that at least some of the copolymer chains were able to escape from acidic organelles. PicoGreen-stained DNA was visible within the cytoplasm, particularly in the perinuclear region of cells following treatment with DNA@G_{55}-(H_{230}-*stat*-M_{30}-*stat*-Rh) but not for the empty G_{55}-(H_{230}-*stat*-M_{30}-*stat*-Rh) control

(**Figure 9 D** & **J**). Multi-fluorescence overlay images clearly show perinuclear accumulation of vesicles, acidic organelles and plasmid DNA, providing evidence for successful intracellular delivery of DNA (**Figure 9 K** and **L)**. However, treatment of cells with DNA@G_{55}-(H_{230}-*stat*-M_{30}) vesicles for 24 h did not result in transfection and expression of mCherry protein (**Figure S15**), whereas the use of commercial lipofectamine transfection reagent produced mCherry-positive cells. This indicates that the plasmid DNA did not cross the nuclear membrane, which is an essential step for transcription. This suggests that DNA@G_{55}-(H_{230}-*stat*-M_{30}-*stat*-Rh) vesicles mainly deliver biomacromolecule cargoes to the cytoplasm. It is also feasible that retention of DNA within intracellular compartments such as late endosomes may limit access to cell nuclei.

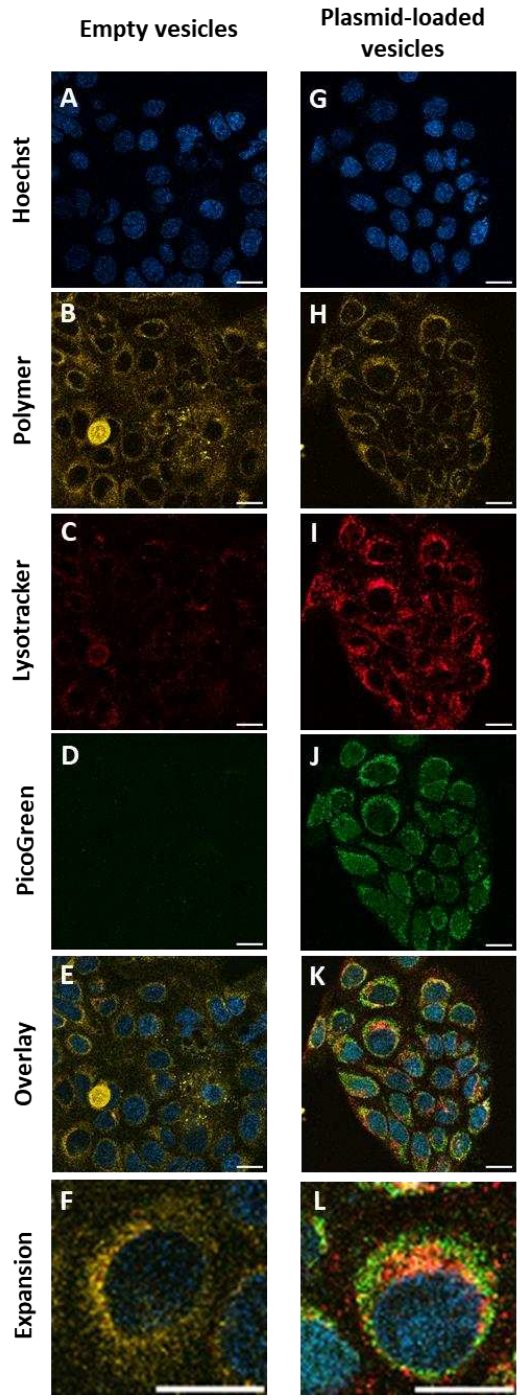

Figure 9. Intracellular DNA delivery using pH-responsive vesicles visualized using confocal microscopy. Rhodamine B-labeled vesicles were treated with PicoGreen to stain their encapsulated DNA payload prior to their addition to FNB6 oral keratinocyte cells. (**A-F**) Cells treated with empty G_{55}-(H_{230}-*stat*-M_{30}-*stat*-Rh) vesicles, (**G-L**) cells treated with DNA-loaded G_{55}-(H_{230}-*stat*-M_{30}-*stat*-Rh) vesicles, (**A** & **G**) Hoechst 33342 nuclear stain, (**B** & **H**) rhodamine B-labeled polymer, (**C** & **I**) Lysotracker deep red lysosomal stain, (**D** & **J**) PicoGreen-stained DNA payload, (**E** & **K**) Overlayed fluorescence images, (**F** & **L**) expanded overlayed fluorescence images. Scale bar = 20 μm in each case.

Discussion

Aqueous PISA formulations have been used to prepare a range of pH-responsive block copolymer nano-objects.[52–56] For example, certain *non-ionic* diblock copolymers can exhibit pH-responsive behavior via either ionization or protonation of carboxylic acid or amine groups located at the end of the steric stabilizer chains.[57–59] More typically, pH-responsive behavior is conferred by targeting a weakly basic block such as poly(2-(diethylamino)ethyl methacrylate) (PDEA) or poly(2-(diisopropylaminoethyl methacrylate) (PDPA).[49] If judiciously combined with a suitable weakly acidic block, this enables the synthesis of so-called 'schizophrenic' diblock copolymers via aqueous PISA.[60] In the specific case of pH-responsive vesicles, Mable et al. reported the design of ABC triblock copolymers in which the C block was PDPA.[61,62] Such vesicles could be efficiently prepared via aqueous PISA and possessed a distinctive framboidal morphology owing to microphase separation within the membrane. More recently, Petrova et al. prepared pH-responsive PDPA-based vesicles using microwave-assisted RAFT aqueous emulsion polymerization[38] while Sumerlin, Gianneschi and co-workers demonstrated that poly(2-(dimethylamino)ethyl methacrylate)-based diblock copolymers prepared via aqueous PISA can form spheres, worms or vesicles depending on the solution pH.[63] Chen et al. prepared redox-sensitive pH-responsive PDPA-based vesicles using cysteine bisacrylamide as a latent crosslinker.[64] However, this latter PISA synthesis was conducted using a 60:40 ethanol/water mixture, which is not suitable for the encapsulation of proteins or nucleic acids.

In this study, PISA was used to prepare G_{55}-(H_{230}-*stat*-M_x) vesicles containing 3.8–14.8 mol% MEMA repeat units. This morpholine-based comonomer was distributed more or less randomly throughout the hydrophobic membrane-forming block. By systematically varying the MEMA content, the critical pH required for vesicle dissociation can be tuned from around pH 3.5 to pH 6.0. Increasing the MEMA content resulted in a relatively modest reduction in the apparent pK_a from 4.3 to 4.8 for the

membrane-forming block. Importantly, vesicle dissociation does not necessarily occur at the pK_a. More specifically, vesicles prepared with relatively low MEMA contents of 3.8 mol% undergo dissociation *below* their apparent pK_a, whereas those containing ≥ 11.1 mol% MEMA dissociate *above* their apparent pK_a. Acid titration curves suggest that this is because the membrane-forming blocks act as a weak polybase, with protonation occurring over a broad pH range and vesicle dissociation only occurring once a certain critical charge density has been achieved. Indeed, aqueous electrophoresis data indicate that such vesicles exhibit slightly positive ζ potentials at pH 6. DLS, NMR, NanoFCM data, and TEM images suggest that vesicle dissociation leads to (mainly) molecularly-dissolved diblock copolymer chains.

Colloidal particles that undergo pH-triggered dissociation in intracellular organelles following endocytosis are of particular interest in the field of nanomedicine.[65] Late endosomes have an internal pH of approximately 5.5, which is lowered to around pH 4.5 following maturation into lysosomes.[66] In principle, vesicle dissociation within these intracellular compartments causes a sudden increase in the osmotic pressure, which ruptures the phospholipid membrane and allows the released payload to escape degradation and enter the cytoplasm.[66,67] Thus vesicle dissociation within this pH range is relevant for intracellular drug delivery. The G_{55}-(H_{230}-*stat*-M_{30}) vesicles meet this criterion while maintaining good colloidal stability at neutral pH. Of particular relevance to our study, Tan et al. previously prepared pH-responsive vesicles loaded with BSA via statistical copolymerization of HPMA with 2-(dimethylamino)ethyl methacrylate (DMAEMA) via aqueous photoinitiated PISA.[68] These vesicles released their BSA payload in response to a CO_2 sparge, which lowers the solution pH, although the precise pH at which this occurred was not reported. Recently, using a PISA formulation involving the same comonomers, Thanapongpibul et al. prepared vesicles loaded with either BSA or ovalbumin that dissociated at pH 6.5.[31] However neither study reported vesicles with *tunable* pH-responsive character. Audureau et al. used PISA to synthesize pH-responsive vesicles by the statistical copolymerization of *N*-cyanomethylacrylamide with acrylic

acid.[69] In contrast to our study, these vesicles were stable at *low* pH and the addition of base caused progressive morphology changes into worms, spheres, and finally into molecularly-dissolved copolymer chains.

There is considerable interest in the therapeutic use of monoclonal antibodies and their F(ab) derivatives owing to their high specificity and relatively low off-target toxicity.[70] Accordingly, biotinylated F(ab) antibody fragment was used as a model functional protein for encapsulation within pH-responsive F(ab)@G_{55}-(H_{230}-*stat*-M_{30}) vesicles and non-responsive F(ab)@G_{55}-H_{230} vesicles during their aqueous PISA synthesis. An encapsulation efficiency of 42 ± 4 % was achieved for F(ab)@G_{55}-(H_{230}-*stat*-M_{30}) vesicles, which is significantly higher than that obtained for well-established methods for loading pH-responsive vesicles reported in the literature.[8,21,24] F(ab)@G_{55}-(H_{230}-*stat*-M_{30}) vesicles undergo dissociation on adjusting the solution pH to (or below) pH 5.25, thus releasing their F(ab) payload. However, compared to ethanol treatment – which is assumed to release the entire payload by fully dissolving the copolymer chains – only approximately 60% of the encapsulated F(ab) was released on lowering the solution pH. We hypothesize that electrostatic interactions occur between the F(ab) and the protonated copolymer chains, which would disrupt antigen binding functionality. Thus it may be beneficial to encapsulate additional excipients to mitigate this problem. It is perhaps worth mentioning that Tan et al. used HPMA and DMAEMA comonomers to encapsulate BSA and reported an encapsulation efficiency of 24 %,[68] whereas Thanapongpibul et al. achieved only 10 %.[31] These lower encapsulation efficiencies are attributed to the lower comonomer concentration compared to that employed in the current study. These two prior studies used either spectroscopic or colorimetric techniques to measure the total amount of released protein, regardless of its conformation. In contrast, the present study demonstrates that a drug-like protein retains its ability to bind to the target ligand after its loading within vesicles and subsequent pH-triggered release.

Plasmid DNA was also efficiently encapsulated during PISA and released by lowering the dispersion pH, which is the first time that this has been reported. When incubated with human oral keratinocytes, DNA@G_{55}-(H_{230}-*stat*-M_{30}-*stat*-Rh) was colocalized with acidic organelles in the perinuclear region (presumably late endosomes or lysosomes), which highlights the potential for the vesicle-mediated intracellular delivery of such biomacromolecules. Similar observations were reported by Thanapongpibul et al when delivering BSA into MCF-7 breast cancer cells using PISA-derived vesicles. Although the vesicles described herein enter the endosomes and subsequently undergo dissociation, the absence of any fluorescent mCherry protein within DNA@G_{55}-(H_{230}-*stat*-M_{30}-*stat*-Rh)-treated cells suggests that (i) the released plasmid DNA does not pass through the nuclear membrane and (ii) transcription of the mCherry reporter gene does not occur. This suggests that such vesicles may be useful for delivery of biomacromolecules to the cytoplasm but not to cell nuclei.

Conclusions

We report the efficient synthesis of new pH-responsive diblock copolymer vesicles under mild conditions using an aqueous PISA formulation. Importantly, the critical pH at which vesicle dissociation occurs can be tuned by systematically varying the copolymer composition. Either biotinylated goat anti-mouse F(ab) or plasmid DNA can be loaded within these vesicles simply by adding such biomacromolecules to the aqueous reaction mixture prior to conducting the PISA synthesis under relatively mild conditions (45 °C in water). This approach leads to encapsulation efficiencies of more than 40% for F(ab) antibody fragments, which is superior to that achieved for traditional vesicle loading methods[8,22–24] and higher than that reported for prior aqueous PISA formulations.[31,68] The diblock copolymer composition of these pH-responsive vesicles has been optimized to undergo dissociation under physiologically relevant conditions, such as those

encountered within the late endosomes of mammalian cells. This aqueous PISA formulation offers a highly versatile platform technology for loading functional biomacromolecules within pH-responsive vesicles for intracellular delivery applications.

Acknowledgments

The authors thank Christopher Hill of the Cryo-Electron Microscopy Facility for his assistance with the electron microscopy and Susan Gauntlett of the Flow Cytometry Core Facility for technical assistance with the NanoFCM. This work was funded by an EPSRC Impact Acceleration Award and UKRI Engineering Biology Mission award (BB/Y007514/1). The authors also acknowledge the BBSRC for funding the acquisition of the NanoFCM (BB/X018989/1).

Conflict of Interest. The authors declare no known conflict of interest.

Supporting Information Available

NMR and GPC data for the PGMA precursor, tabulated reagent masses for synthesis protocols, additional NMR, GPC, TEM and DLS data for $PGMA_{55}$-P($HPMA_{230}$-*stat*-$MEMA_x$) copolymer vesicles, acid titration curves for $PGMA_{55}$-P($HPMA_{230}$-*stat*-$MEMA_x$) copolymer vesicles, digital photographs of $PGMA_{55}$-P($HPMA_{230}$-*stat*-$MEMA_{30}$) in two pH buffers, NMR and GPC data for F(ab)-loaded $PGMA_{55}$-P($HPMA_{230}$-*stat*-$MEMA_{30}$) vesicles, preparative SEC data obtained for Texas Red-labeled F(ab)-loaded vesicles and empty vesicles, fluorescence microscopy images recorded for attempted transfection of FNB6 cells using DNA-loaded G_{55}-(H_{230}-*stat*-M_{30}) vesicles.

References

(1) Blanazs, A.; Armes, S. P.; Ryan, A. J. Self-Assembled Block Copolymer Aggregates: From Micelles to Vesicles and Their Biological Applications. *Macromol. Rapid Commun.* **2009**, *30* (4–5), 267–277. https://doi.org/10.1002/marc.200800713.

(2) Du, J.; O'Reilly, R. K. Advances and Challenges in Smart and Functional Polymer Vesicles. *Soft Matter* **2009**, *5* (19), 3544–3561. https://doi.org/10.1039/b905635a.

(3) Discher, B. M.; Won, Y.-Y.; Ege, D. S.; Lee, J. C. M.; Bates, F. S.; Discher, D. E.; Hammer, D. A. Polymersomes: Tough Vesicles Made from Diblock Copolymers. *Science.* **1999**, *284* (5417), 1143–1146. https://doi.org/10.1126/science.284.5417.1143.

(4) Vriezema, D. M.; Garcia, P. M. L.; Sancho Oltra, N.; Hatzakis, N. S.; Kuiper, S. M.; Nolte, R. J. M.; Rowan, A. E.; Van Hest, J. C. M. Positional Assembly of Enzymes in Polymersome Nanoreactors for Cascade Reactions. *Angew. Chemie - Int. Ed.* **2007**, *46* (39), 7378–7382. https://doi.org/10.1002/anie.200701125.

(5) Ooi, Y. J.; Huang, C.; Lau, K.; Chew, S. Y.; Park, J. G.; Chan-Park, M. B. Nontoxic, Biodegradable Hyperbranched Poly(β-Amino Ester)s for Efficient SiRNA Delivery and Gene Silencing. *ACS Appl. Mater. Interfaces* **2024**, *16* (11), 14093–14112. https://doi.org/10.1021/acsami.3c10620.

(6) Hu, X.; Zhang, Y.; Xie, Z.; Jing, X.; Bellotti, A.; Gu, Z. Stimuli-Responsive Polymersomes for Biomedical Applications. *Biomacromolecules* **2017**, *18* (3), 649–673. https://doi.org/10.1021/acs.biomac.6b01704.

(7) Du, J.; Tang, Y.; Lewis, A. L.; Armes, S. P. PH-Sensitive Vesicles Based on a Biocompatible Zwitterionic Diblock Copolymer. *J. Am. Chem. Soc.* **2005**, *127* (51), 17982–17983. https://doi.org/10.1021/ja056514l.

(8) Lomas, H.; Canton, I.; MacNeil, S.; Du, J.; Armes, S. P.; Ryan, A. J.; Lewis, A. L.; Battaglia, G. Biomimetic PH Sensitive Polymersomes for Efficient DNA Encapsulation and Delivery. *Adv. Mater.* **2007**, *19* (23), 4238–4243. https://doi.org/10.1002/adma.200700941.

(9) Fonseca, M.; Jarak, I.; Victor, F.; Domingues, C.; Veiga, F.; Figueiras, A. Polymersomes as the Next Attractive Generation of Drug Delivery Systems: Definition, Synthesis and Applications. *Materials.* **2024**, *17* (2), 319. https://doi.org/10.3390/ma17020319.

(10) Ahmed, F.; Discher, D. E. Self-Porating Polymersomes of PEG-PLA and PEG-PCL: Hydrolysis-Triggered Controlled Release Vesicles. *J. Control. Release* **2004**, *96* (1), 37–53. https://doi.org/10.1016/j.jconrel.2003.12.021.

(11) Brinkhuis, R. P.; Rutjes, F. P. J. T.; Van Hest, J. C. M. Polymeric Vesicles in Biomedical Applications. *Polym. Chem.* **2011**, *2* (7), 1449–1462. https://doi.org/10.1039/c1py00061f.

(12) Iqbal, S.; Blenner, M.; Alexander-Bryant, A.; Larsen, J. Polymersomes for Therapeutic Delivery of Protein and Nucleic Acid Macromolecules: From Design to Therapeutic Applications. *Biomacromolecules* **2020**, *21* (4), 1327–1350. https://doi.org/10.1021/acs.biomac.9b01754.

(13) Matoori, S.; Leroux, J. C. Twenty-Five Years of Polymersomes: Lost in Translation? *Mater. Horizons* **2020**, *7* (5), 1297–1309. https://doi.org/10.1039/c9mh01669d.

(14) Colley, H. E.; Hearnden, V.; Avila-Olias, M.; Cecchin, D.; Canton, I.; Madsen, J.; Macneil, S.; Warren, N.; Hu, K.; McKeating, J. A.; Armes, S. P.; Murdoch, C.; Thornhill, M. H.; Battaglia, G. Polymersome-Mediated Delivery of Combination Anticancer Therapy to Head and Neck Cancer Cells: 2D and 3D in Vitro Evaluation. *Mol. Pharm.* **2014**, *11* (4), 1176–1188. https://doi.org/10.1021/mp400610b.

(15) Dinu, M. V.; Dinu, I. A.; Saxer, S. S.; Meier, W.; Pieles, U.; Bruns, N. Stabilizing Enzymes within Polymersomes by Coencapsulation of Trehalose. *Biomacromolecules* **2021**, *22* (1), 134–145. https://doi.org/10.1021/acs.biomac.0c00824.

(16) Lefley, J.; Waldron, C.; Becer, C. R. Macromolecular Design and Preparation of Polymersomes. *Polym. Chem.* **2020**, *11* (45), 7124–7136. https://doi.org/10.1039/d0py01247e.

(17) Hua, C.; Qiu, L. Polymersomes for Therapeutic Protein and Peptide Delivery: Towards Better Loading Properties. *Int. J. Nanomedicine* **2024**, *19*, 2317–2340. https://doi.org/10.2147/IJN.S444910.

(18) Xiong, X. Y.; Li, Y. P.; Li, Z. L.; Zhou, C. L.; Tam, K. C.; Liu, Z. Y.; Xie, G. X. Vesicles from Pluronic/Poly(Lactic Acid) Block Copolymers as New Carriers for Oral Insulin Delivery. *J. Control. Release* **2007**, *120* (1–2), 11–17. https://doi.org/10.1016/j.jconrel.2007.04.004.

(19) Sanson, C.; Diou, O.; Thévenot, J.; Ibarboure, E.; Soum, A.; Brûlet, A.; Miraux, S.; Thiaudière, E.; Tan, S.; Brisson, A.; Dupuis, V.; Sandre, O.; Lecommandoux, S. Doxorubicin Loaded Magnetic Polymersomes: Theranostic Nanocarriers for MR Imaging and Magneto-Chemotherapy. *ACS Nano* **2011**, *5* (2), 1122–1140. https://doi.org/10.1021/nn102762f.

(20) Schatz, C.; Louguet, S.; Meins, J. F. Le; Lecommandoux, S. Polysaccharide-Block-Polypeptide Copolymer Vesicles: Towards Synthetic Viral Capsids. *Angew. Chemie - Int. Ed.* **2009**, *48* (14), 2572–2575. https://doi.org/10.1002/anie.200805895.

(21) Contini, C.; Pearson, R.; Wang, L.; Messager, L.; Gaitzsch, J.; Rizzello, L.; Ruiz-Perez, L.; Battaglia, G. Bottom-Up Evolution of Vesicles from Disks to High-Genus Polymersomes. *iScience* **2018**, *7*, 132–144. https://doi.org/10.1016/j.isci.2018.08.018.

(22) Chierico, L. Polymersomes Mediated Intracellular Delivery of Antibodies: Implication in Anticancer Therapy., PhD Thesis, University College London, 2015.

(23) Canton, I.; Massignani, M.; Patikarnmonthon, N.; Chierico, L.; Robertson, J.; Renshaw, S. A.; Warren, N. J.; Madsen, J. P.; Armes, S. P.; Lewis, A. L.; Battaglia, G. Fully Synthetic Polymer Vesicles for Intracellular Delivery of Antibodies in Live Cells. *FASEB J.* **2013**, *27* (1), 98–108. https://doi.org/10.1096/fj.12-212183.

(24) Wang, L.; Chierico, L.; Little, D.; Patikarnmonthon, N.; Yang, Z.; Azzouz, M.; Madsen, J.; Armes, S. P.; Battaglia, G. Encapsulation of Biomacromolecules within Polymersomes by Electroporation. *Angew. Chemie* **2012**, *124* (44), 11284–11287. https://doi.org/10.1002/ange.201204169.

(25) Patikarnmonthon, N. Optimisation of Polymersomes Preparation and SiRNA Encapsulation, PhD Thesis, University of Sheffield, 2013.

(26) Canning, S. L.; Smith, G. N.; Armes, S. P. A Critical Appraisal of RAFT-Mediated Polymerization-Induced Self-Assembly. *Macromolecules* **2016**, *49* (6), 1985–2001. https://doi.org/10.1021/acs.macromol.5b02602.

(27) D'Agosto, F.; Rieger, J.; Lansalot, M. RAFT-Mediated Polymerization-Induced Self-Assembly. *Angew. Chemie - Int. Ed.* **2020**, *59* (22), 8368–8392. https://doi.org/10.1002/anie.201911758.

(28) Warren, N. J.; Armes, S. P. Polymerization-Induced Self-Assembly of Block Copolymer Nano-Objects via RAFT Aqueous Dispersion Polymerization. *J. Am. Chem. Soc.* **2014**, *136* (29), 10174–10185. https://doi.org/10.1021/ja502843f.

(29) Blanazs, A.; Ryan, A. J.; Armes, S. P. Predictive Phase Diagrams for RAFT Aqueous Dispersion Polymerization: Effect of Block Copolymer Composition, Molecular Weight, and Copolymer Concentration. *Macromolecules* **2012**, *45* (12), 5099–5107. https://doi.org/10.1021/ma301059r.

(30) Phan, H.; Cossutta, M.; Houppe, C.; Le Cœur, C.; Prevost, S.; Cascone, I.; Courty, J.; Penelle, J.; Couturaud, B. Polymerization-Induced Self-Assembly (PISA) for in Situ Drug Encapsulation or Drug Conjugation in Cancer Application. *J. Colloid Interface Sci.* **2022**, *618*, 173–184. https://doi.org/10.1016/j.jcis.2022.03.044.

(31) Thanapongpibul, C.; Rifaie-Graham, O.; Ojansivu, M.; Najer, A.; Kim, H.; Bakker, S. E.; Chami, M.; Peeler, D. J.; Liu, C.; Yeow, J.; Stevens, M. M. Unlocking Intracellular Protein Delivery by Harnessing Polymersomes Synthesized at Microliter Volumes Using Photo-PISA. *Adv. Mater.* **2024**, *2408000*. https://doi.org/10.1002/adma.202408000.

(32) Edmans, J. G.; Harrison, S.; Hatton, P. V.; Murdoch, C.; Spain, S. G.; Colley, H. E. Electrospinning Polymersomes into Bead-on-String Polyethylene Oxide Fibres for the Delivery of Biopharmaceuticals to Mucosal Epithelia. *Biomater. Adv.* **2024**, *157*, 213734. https://doi.org/10.1016/j.bioadv.2023.213734.

(33) Phan, H.; Taresco, V.; Penelle, J.; Couturaud, B. Polymerisation-Induced Self-Assembly (PISA) as a Straightforward Formulation Strategy for Stimuli-Responsive Drug Delivery Systems and Biomaterials: Recent Advances. *Biomater. Sci.* **2021**, *9* (1), 38–50. https://doi.org/10.1039/d0bm01406k.

(34) Mable, C. J.; Gibson, R. R.; Prevost, S.; McKenzie, B. E.; Mykhaylyk, O. O.; Armes, S. P. Loading of Silica Nanoparticles in Block Copolymer Vesicles during Polymerization-Induced Self-Assembly: Encapsulation Efficiency and Thermally

Triggered Release. *J. Am. Chem. Soc.* **2015**, *137* (51), 16098–16108. https://doi.org/10.1021/jacs.5b10415.

(35) Tan, J.; Sun, H.; Yu, M.; Sumerlin, B. S.; Zhang, L. Photo-PISA: Shedding Light on Polymerization-Induced Self-Assembly. *ACS Macro Lett.* **2015**, *4* (11), 1249–1253. https://doi.org/10.1021/acsmacrolett.5b00748.

(36) Blackman, L. D.; Varlas, S.; Arno, M. C.; Fayter, A.; Gibson, M. I.; O'Reilly, R. K. Permeable Protein-Loaded Polymersome Cascade Nanoreactors by Polymerization-Induced Self-Assembly. *ACS Macro Lett.* **2017**, *6* (11), 1263–1267. https://doi.org/10.1021/acsmacrolett.7b00725.

(37) Czajka, A.; Byard, S. J.; Armes, S. P. Silica Nanoparticle-Loaded Thermoresponsive Block Copolymer Vesicles: A New Post-Polymerization Encapsulation Strategy and Thermally Triggered Release. *Chem. Sci.* **2022**, *13* (33), 9569–9579. https://doi.org/10.1039/d2sc02103j.

(38) Lukáš Petrova, S.; Sincari, V.; Konefał, R.; Pavlova, E.; Hrubý, M.; Pokorný, V.; Jäger, E. Microwave Irradiation-Assisted Reversible Addition-Fragmentation Chain Transfer Polymerization-Induced Self-Assembly of PH-Responsive Diblock Copolymer Nanoparticles. *ACS Omega* **2022**, *7* (47), 42711–42722. https://doi.org/10.1021/acsomega.2c04036.

(39) He, J.; Cao, J.; Chen, Y.; Zhang, L.; Tan, J. Thermoresponsive Block Copolymer Vesicles by Visible Light-Initiated Seeded Polymerization-Induced Self-Assembly for Temperature-Regulated Enzymatic Nanoreactors. *ACS Macro Lett.* **2020**, *9* (4), 533–539. https://doi.org/10.1021/acsmacrolett.0c00151.

(40) Blackman, L. D.; Varlas, S.; Arno, M. C.; Houston, Z. H.; Fletcher, N. L.; Thurecht, K. J.; Hasan, M.; Gibson, M. I.; O'Reilly, R. K. Confinement of Therapeutic Enzymes in Selectively Permeable Polymer Vesicles by Polymerization-Induced Self-Assembly (PISA) Reduces Antibody Binding and Proteolytic Susceptibility. *ACS Cent. Sci.* **2018**, *4* (6), 718–723. https://doi.org/10.1021/acscentsci.8b00168.

(41) Patel, P.; Ibrahim, N. M.; Cheng, K. The Importance of Apparent PKa in the Development of Nanoparticles Encapsulating SiRNA and MRNA. *Trends Pharmacol. Sci.* **2021**, *42* (6), 448–460. https://doi.org/10.1016/j.tips.2021.03.002.

(42) Schneider, C. A.; Rasband, W. S.; Eliceiri, K. W. NIH Image to ImageJ: 25 Years of Image Analysis. *Nat. Methods* **2012**, *9* (7), 671–675. https://doi.org/10.1038/nmeth.2089.

(43) Edmans, J. G.; Ollington, B.; Colley, H. E.; Santocildes-Romero, M. E.; Madsen, L. S.; Hatton, P. V; Murdoch, C. Electrospun Patch Delivery of Anti-TNF α F(Ab) for the Treatment of Inflammatory Oral Mucosal Disease. *J. Control. Release* **2022**, *350*, 146–157. https://doi.org/10.1016/j.jconrel.2022.08.016.

(44) Leung, A. K. K.; Tam, Y. Y. C.; Chen, S.; Hafez, I. M.; Cullis, P. R. Microfluidic Mixing: A General Method for Encapsulating Macromolecules in Lipid Nanoparticle Systems. *J. Phys. Chem. B* **2015**, *119* (28), 8698–8706. https://doi.org/10.1021/acs.jpcb.5b02891.

(45) Jennings, L. R.; Colley, H. E.; Ong, J.; Panagakos, F.; Masters, J. G.; Trivedi, H. M.; Murdoch, C.; Whawell, S. Development and Characterization of *In Vitro* Human Oral Mucosal Equivalents Derived from Immortalized Oral Keratinocytes. *Tissue Eng. Part C Methods* **2016**, *22* (12), 1108–1117. https://doi.org/10.1089/ten.tec.2016.0310.

(46) Blanazs, A.; Madsen, J.; Battaglia, G.; Ryan, A. J.; Armes, S. P. Mechanistic Insights for Block Copolymer Morphologies: How Do Worms Form Vesicles? *J. Am. Chem. Soc.* **2011**, *133* (41), 16581–16587. https://doi.org/10.1021/ja206301a.

(47) Stetefeld, J.; McKenna, S. A.; Patel, T. R. Dynamic Light Scattering: A Practical Guide and Applications in Biomedical Sciences. *Biophys. Rev.* **2016**, *8* (4), 409–427. https://doi.org/10.1007/s12551-016-0218-6.

(48) North, S. M.; Armes, S. P. Synthesis of Polyampholytic Diblock Copolymers: Via RAFT Aqueous Solution Polymerization. *Polym. Chem.* **2021**, *12* (33), 4846–4855. https://doi.org/10.1039/d1py01020d.

(49) Bütün, V.; Armes, S. P.; Billingham, N. C. Synthesis and Aqueous Solution Properties of Near-Monodisperse Tertiary Amine Methacrylate Homopolymers and Diblock Copolymers. *Polymer (Guildf).* **2001**, *42* (14), 5993–6008. https://doi.org/10.1016/S0032-3861(01)00066-0.

(50) Save, M.; Weaver, J. V. M.; Armes, S. P.; McKenna, P. Atom Transfer Radical Polymerization of Hydroxy-Functional Methacrylates at Ambient Temperature:

Comparison of Glycerol Monomethacrylate with 2-Hydroxypropyl Methacrylate. *Macromolecules* **2002**, *35* (4), 1152–1159. https://doi.org/10.1021/ma011541r.

(51) Ratcliffe, L. P. D.; Blanazs, A.; Williams, C. N.; Brown, S. L.; Armes, S. P. RAFT Polymerization of Hydroxy-Functional Methacrylic Monomers under Heterogeneous Conditions: Effect of Varying the Core-Forming Block. *Polym. Chem.* **2014**, *5* (11), 3643–3655. https://doi.org/10.1039/c4py00203b.

(52) Pei, Y.; Lowe, A. B.; Roth, P. J. Stimulus-Responsive Nanoparticles and Associated (Reversible) Polymorphism via Polymerization Induced Self-Assembly (PISA). *Macromol. Rapid Commun.* **2017**, *38* (1), 1–14. https://doi.org/10.1002/marc.201600528.

(53) Xu, X. F.; Pan, C. Y.; Zhang, W. J.; Hong, C. Y. Polymerization-Induced Self-Assembly Generating Vesicles with Adjustable PH-Responsive Release Performance. *Macromolecules* **2019**, *52* (5), 1965–1975. https://doi.org/10.1021/acs.macromol.9b00144.

(54) Zhang, F.; Niu, Y.; Li, Y.; Yao, Q.; Chen, X.; Zhou, H.; Zhou, M.; Xiao, J. Fabrication and Characterization of Structurally Stable PH-Responsive Polymeric Vesicles by Polymerization-Induced Self-Assembly. *RSC Adv.* **2021**, *11* (46), 29042–29051. https://doi.org/10.1039/d1ra05555k.

(55) Du, R.; Fielding, L. A. PH-Responsive Nanogels Generated by Polymerization-Induced Self-Assembly of a Succinate-Functional Monomer. *Macromolecules* **2024**, *57* (8), 3496–3501. https://doi.org/10.1021/acs.macromol.4c00427.

(56) Zhao, X.; Chen, M.; Zhang, W. G.; Wang, C. H.; Wang, F.; You, Y. Z.; Zhang, W. J.; Hong, C. Y. Polymerization-Induced Self-Assembly to Produce Prodrug Nanoparticles with Reduction-Responsive Camptothecin Release and PH-Responsive Charge-Reversible Property. *Macromol. Rapid Commun.* **2020**, *41* (15), 1–8. https://doi.org/10.1002/marc.202000260.

(57) Lovett, J. R.; Warren, N. J.; Ratcliffe, L. P. D.; Kocik, M. K.; Armes, S. P. PH-Responsive Non-Ionic Diblock Copolymers: Ionization of Carboxylic Acid End-Groups Induces an Order-Order Morphological Transition. *Angew. Chemie - Int. Ed.* **2015**, *54* (4), 1279–1283. https://doi.org/10.1002/anie.201409799.

(58) Penfold, N. J. W.; Lovett, J. R.; Warren, N. J.; Verstraete, P.; Smets, J.; Armes, S. P. PH-Responsive Non-Ionic Diblock Copolymers: Protonation of a Morpholine End-Group Induces an Order–Order Transition. *Polym. Chem.* **2016**, *7* (1), 79–88. https://doi.org/10.1039/C5PY01510C.

(59) Deane, O. J.; Jennings, J.; Armes, S. P. Shape-Shifting Thermoreversible Diblock Copolymer Nano-ObjectsviaRAFT Aqueous Dispersion Polymerization of 4-Hydroxybutyl Acrylate. *Chem. Sci.* **2021**, *12* (41), 13719–13729. https://doi.org/10.1039/d1sc05022b.

(60) North, S. M.; Armes, S. P. One-Pot Synthesis and Aqueous Solution Properties of PH-Responsive Schizophrenic Diblock Copolymer Nanoparticles Prepared via RAFT Aqueous Dispersion Polymerization. *Polym. Chem.* **2021**, *12* (40), 5842–5850. https://doi.org/10.1039/d1py01114f.

(61) Mable, C. J.; Fielding, L. A.; Derry, M. J.; Mykhaylyk, O. O.; Chambon, P.; Armes, S. P. Synthesis and PH-Responsive Dissociation of Framboidal ABC Triblock Copolymer Vesicles in Aqueous Solution. *Chem. Sci.* **2018**, *9* (6), 1454–1463. https://doi.org/10.1039/c7sc04788f.

(62) Mable, C. J.; Canton, I.; Mykhaylyk, O. O.; Ustbas Gul, B.; Chambon, P.; Themistou, E.; Armes, S. P. Targeting Triple-Negative Breast Cancer Cells Using Dengue Virus-Mimicking PH-Responsive Framboidal Triblock Copolymer Vesicles. *Chem. Sci.* **2019**, *10* (18), 4811–4821. https://doi.org/10.1039/c8sc05589k.

(63) Bowman, J. I.; Eades, C. B.; Korpanty, J.; Garrison, J. B.; Scheutz, G. M.; Goodrich, S. L.; Gianneschi, N. C.; Sumerlin, B. S. Controlling Morphological Transitions of Polymeric Nanoparticles via Doubly Responsive Block Copolymers. *Macromolecules* **2023**, *56* (9), 3316–3323. https://doi.org/10.1021/acs.macromol.3c00445.

(64) Chen, M.; Li, J. W.; Zhang, W. J.; Hong, C. Y.; Pan, C. Y. PH- and Reductant-Responsive Polymeric Vesicles with Robust Membrane-Cross-Linked Structures: In Situ Cross-Linking in Polymerization-Induced Self-Assembly. *Macromolecules* **2019**, *52* (3), 1140–1149. https://doi.org/10.1021/acs.macromol.8b02081.

(65) Liu, J.; Huang, Y.; Kumar, A.; Tan, A.; Jin, S.; Mozhi, A.; Liang, X. J. PH-Sensitive Nano-Systems for Drug Delivery in Cancer Therapy. *Biotechnol. Adv.* **2014**, *32* (4),

693–710. https://doi.org/10.1016/j.biotechadv.2013.11.009.

(66) Canton, I.; Battaglia, G. Endocytosis at the Nanoscale. *Chem. Soc. Rev.* **2012**, *41* (7), 2718. https://doi.org/10.1039/c2cs15309b.

(67) Vermeulen, L. M. P.; De Smedt, S. C.; Remaut, K.; Braeckmans, K. The Proton Sponge Hypothesis: Fable or Fact? *Eur. J. Pharm. Biopharm.* **2018**, *129*, 184–190. https://doi.org/10.1016/j.ejpb.2018.05.034.

(68) Tan, J.; Zhang, X.; Liu, D.; Bai, Y.; Huang, C.; Li, X.; Zhang, L. Facile Preparation of CO2-Responsive Polymer Nano-Objects via Aqueous Photoinitiated Polymerization-Induced Self-Assembly (Photo-PISA). *Macromol. Rapid Commun.* **2017**, *38* (13), 1–8. https://doi.org/10.1002/marc.201600508.

(69) Audureau, N.; Coumes, F.; Guigner, J. M.; Guibert, C.; Stoffelbach, F.; Rieger, J. Dual Thermo- and PH-Responsive N-Cyanomethylacrylamide-Based Nano-Objects Prepared by RAFT-Mediated Aqueous Polymerization-Induced Self-Assembly. *Macromolecules* **2022**, *55* (24), 10993–11005. https://doi.org/10.1021/acs.macromol.2c01953.

(70) Carter, P. J.; Lazar, G. A. Next Generation Antibody Drugs: Pursuit of the “High-Hanging Fruit.” *Nat. Rev. Drug Discov.* **2018**, *17* (3), 197–223. https://doi.org/10.1038/nrd.2017.227.